

1 Far field tsunami simulations of the 1755 Lisbon earthquake: Implications
2 for tsunami hazard to the U.S. East Coast and the Caribbean

3
4 Roy Barkan^a, Uri ten Brink^{b,*}, Jian Lin^c

5
6 ^a *Department of Geophysics and Planetary Sciences, Tel Aviv University, Ramat Aviv,*
7 *Tel-Aviv 69978, Israel*

8 ^b *U.S. Geological Survey, Woods Hole, MA 02543, USA*

9 ^c *Department of Geology and Geophysics, Woods Hole Oceanographic Institution,*
10 *Woods Hole, MA 02543, USA*

11
12 * Corresponding author: Uri ten Brink, USGS Woods Hole Science Center, 384 Woods
13 Hole Rd., Woods Hole, MA 02543 USA. Tel: +1-508-457-2396 ; Fax: +1-508-457-
14 2310 *E-mail address:* utenbrink@usgs.gov

15
16 **Abstract**

17 The great Lisbon earthquake of November 1st, 1755 with an estimated moment
18 magnitude of 8.5-9.0 was the most destructive earthquake in European history. The
19 associated tsunami run-up was reported to have reached 5-15 m along the Portuguese and
20 Moroccan coasts and the run-up was significant at the Azores and Madeira Island. Run-
21 up reports from a trans-oceanic tsunami were documented in the Caribbean, Brazil and
22 Newfoundland (Canada). No reports were documented along the U.S. East Coast. Many
23 attempts have been made to characterize the 1755 Lisbon earthquake source using
24 geophysical surveys and modeling the near-field earthquake intensity and tsunami
25 effects. Studying far field effects, as presented in this paper, is advantageous in
26 establishing constraints on source location and strike orientation because trans-oceanic
27 tsunamis are less influenced by near source bathymetry and are unaffected by triggered
28 submarine landslides at the source. Source location, fault orientation and bathymetry are
29 the main elements governing transatlantic tsunami propagation to sites along the U.S.
30 East Coast, much more than distance from the source and continental shelf width. Results
31 of our far and near-field tsunami simulations based on relative amplitude comparison

32 limit the earthquake source area to a region located south of the Gorringe Bank in the
33 center of the Horseshoe Plain. This is in contrast with previously suggested sources such
34 as Marqués de Pombal Fault, and Gulf of Cádiz Fault, which are farther east of the
35 Horseshoe Plain. The earthquake was likely to be a thrust event on a fault striking $\sim 345^\circ$
36 and dipping to the ENE as opposed to the suggested earthquake source of the Gorringe
37 Bank Fault, which trends NE-SW. Gorringe Bank, the Madeira-Tore Rise (MTR), and the
38 Azores appear to have acted as topographic scatterers for tsunami energy, shielding most
39 of the U.S. East Coast from the 1755 Lisbon tsunami. Additional simulations to assess
40 tsunami hazard to the U.S. East Coast from possible future earthquakes along the Azores-
41 Iberia plate boundary indicate that sources west of the MTR and in the Gulf of Cadiz may
42 affect the southeastern coast of the U.S. The Azores-Iberia plate boundary west of the
43 MTR is characterized by strike-slip faults, not thrusts, but the Gulf of Cadiz may have
44 thrust faults. Southern Florida seems to be at risk from sources located east of MTR and
45 South of the Gorringe Bank, but it is mostly shielded by the Bahamas. The Gulf of Cádiz
46 is another source area of potential tsunami hazard to the U.S. East Coast. Higher
47 resolution near-shore bathymetry along the U.S. East Coast and the Caribbean as well as
48 a detailed study of potential tsunami sources in the central west part of the Horseshoe
49 Plain are necessary to verify our simulation results.

50

51 *Keywords:* tsunami modeling, 1755 Lisbon earthquake, Azores-Gibraltar plate boundary,
52 U.S. East Coast, Caribbean tsunami

53

54 **1. Introduction**

55 The Azores-Gibraltar plate boundary is the source of the largest earthquakes and
56 tsunamis in the north Atlantic basin. These include the 1941 M8.4 and 1975 M1979
57 strike-slip earthquakes west of the Madeira-Tore Rise (MTR) and the 1969, Ms 8.0
58 earthquake in the Horseshoe Plain south-east of the Gorringe Bank (Buforn et al., 1988;
59 2004; Fukao, 1973) (Fig. 1). This plate boundary is also believed to have been the source
60 region of the 1722 and 1761 tsunamigenic earthquakes (Baptista et al., 2006) and of the
61 great November 1st, 1755 Lisbon earthquake (Machado, 1966; Moreira, 1985; Johnston,
62 1996). The earthquake, which was estimated to be of magnitude Mw 8.5-9.0 (e.g.,
63 Gutscher et al., 2006), had the largest documented felt area of any shallow earthquake in

64 Europe (Martinez-Solares et al., 1979; Johnston 1996) and was the largest natural disaster
65 to have affected Europe in the past 500 years. It inflicted up to 100,000 deaths (Chester,
66 2001) through destruction by ground shaking, ensuing fires and tsunami waves of 5-15 m
67 that devastated the coasts of Southwest Iberia and Northwest Morocco and were even
68 reported as far north as Cornwall, England (Baptista et al., 1998a). Additionally, Grácia
69 et al. (2003a,b) showed clear evidence of submarine landslide deposits from acoustic-
70 backscattering, suggesting that the slope failure process could have contributed to
71 tsunami generation and reports of tsunami waves along the European and Moroccan
72 coasts.

73 The large tsunami-wave generated by the earthquake also caused damage in the
74 eastern Lesser Antilles, as far north as Newfoundland, Canada and as far south as Brazil
75 (Kozak et al., 2005; Ruffman, 2006). However, no reports were documented from cities
76 along the U.S. East Coast (Reid, 1914; Lockridge et al., 2002; Ruffman, 2006). Table 1
77 summarizes the tsunami run-up reports from around the Atlantic Ocean (Reid, 1914;
78 Ruffman, 1990, 2006; Baptista et al., 1998a; O'Loughlin and Lander, 2003; Kozak et al.,
79 2005). Fig. 2 shows relevant locations on the map as well as cities along the U.S. East
80 Coast, which existed in 1755.

81 Although many attempts have been made to characterize the 1755 Lisbon earthquake
82 and tsunami (Johnston 1996; Baptista et al., 1998a,b; Gutscher et al., 2006; Grandin et al.,
83 2007) only one study (Mader, 2001) had considered the far field effects of the tsunami.
84 Studying far field effects is advantageous in determining a possible source location and
85 fault orientation because such effects are less influenced by near-source bathymetry and
86 are unaffected by components of the tsunami wavefield generated by submarine
87 landslides which are significant in the near-field (Gisler et al., 2006), but attenuate
88 rapidly. Mader (2001) generated a numerical model for a source centered at the location
89 of the Mw 7.8, 1969 earthquake (Fig. 1), which provided estimates of the deep water
90 wave amplitudes along the U.S. East Coast and the Caribbean. However, the study did
91 not attempt to characterize the earthquake's source parameters, using instead a 30-m
92 vertical drop of a 300-km radius area as a source; nor did it endeavor to compare tsunami
93 hazard along the U.S. East Coast and the Caribbean from different sources in the region.

94 In this study we first investigate constraints on the epicenter of the 1755 Lisbon
95 earthquake from far field numerical tsunami simulations. Second, features such as fault

96 orientation, distance from source, and near-source and regional bathymetry are tested in
97 order to determine what governs tsunami propagation in the Atlantic Ocean. We then
98 assess the tsunami hazard to the U.S. East Coast and the Caribbean from possible future
99 earthquake sources located in the east Atlantic region.

100

101 **2. Tectonic setting and the 1755 Lisbon earthquake**

102 The eastern end of the Azores-Gibraltar plate boundary, which separates the Eurasian
103 and African plates, is a region of complex bathymetry. Plate kinematic models together
104 with focal mechanisms show that the motion between the two plates is slow (0.7-5
105 mm/yr) (Argus et al. 1989; Nocquet and Calais, 2004; Fernandes et al, 2007), changing
106 along the boundary from extension in the Azores to compression towards the east that
107 includes the Gorringe Bank and the Gibraltar arc (Fig. 1, inset). The precise location of
108 the plate boundary close to Iberia is uncertain and the plate boundary deformation there
109 might be diffuse over a 200-330 km wide zone (Grimison and Chen, 1986; Hayward et
110 al., 1999). The dominant active structures in this region are the Gorringe Bank Fault
111 (GBF), the Marqués de Pombal Fault (MPF), the St. Vincente Fault (SVF) and the
112 Horseshoe Fault (HSF), which have been studied by several authors (Sartori et al., 1994;
113 Baptista et. al., 2003; Grácia et al., 2003a; Terrinha et al., 2003). These structures and
114 most of the faults in this area trend NE-SW (Borges et al., 2001; Zitellini et al., 2004;
115 Buforn et al., 2004) (Fig. 1).

116 Thus far the source of the great Lisbon earthquake remains unknown (Gutscher,
117 2004). A consensus attributed the origin of the earthquake to a structure located between
118 the Gorringe Bank and the Coral Patch Ridge (Machado, 1966; Moreira, 1985; Johnston,
119 1996) (Fig. 1). Yet the relatively modest surface area of this fault region makes it difficult
120 to explain the high seismic moment of $\sim 2 \times 10^{22}$ Nm, for a reasonable set of fault
121 parameters (e.g., co-seismic displacement, rigidity, and recurrence) (Gutscher et al.,
122 2006). Three major solutions were proposed based on seismic reflection and multibeam
123 echosounder data, estimates of shaking intensity, and backward ray tracing of tsunami
124 propagation. These fault solutions are shown in Fig. 1 and will be referred later in this
125 paper as:

126 Gorringe Bank Fault (GBF) – Johnston (1996) and Grandin et al. (2007) suggested a NE-
127 SW trending thrust fault (strike 060°), possibly outcropping at the base of the NW
128 flank of the Gorringe Bank.
129 Marqués de Pombal Fault (MPF) – Zitellini et al. (2001) and Grácia et al. (2003a)
130 suggested active thrusting along the MPF, located 80 km west of Cape Sao Vicente
131 (strike 020°).
132 Gulf of Cádiz Fault (GCF) – Gutscher et al. (2002, 2006) and Thiebot and Gutscher
133 (2006) proposed a fault plane in the western Gulf of Cádiz, possibly as part of an
134 African plate subduction beneath Gibraltar (strike 349°).

135

136 **3. Methodology**

137 *3.1 Tsunami model simulations*

138 All simulations presented in this study were generated using COMCOT (Cornell
139 Multi-grid Coupled Tsunami Model) developed by P.L.-F. Liu, X. Wang, S.-B. Woo, Y-
140 S. Cho, and S.B. Yoon, at the School of Civil and Environmental Engineering, Cornell
141 University (Liu et al., 1998). All calculations were performed on the Arctic Region
142 Supercomputing Center in Alaska, using the Tsunami Computational Portal at:
143 <http://tsunamiportal.nacse.org/wizard.php>. COMCOT solves both linear shallow water
144 (LSW) and non-linear shallow water (NLSW) equations in spherical coordinates. Two
145 simplifying assumptions were made to create the initial sea surface deformation, which
146 serve as the initial boundary conditions for the numerical simulations. First, the sea
147 surface responds instantaneously to seafloor earthquake deformation. Second, the initial
148 sea surface displacement is identical to that of the seafloor (Ruff, 2003). The initial sea
149 surface deformation, computed based upon user-provided fault parameters, is identical
150 to the seafloor displacement generated by Coulomb 3.0 (Lin and Stein, 2004; Toda et al.,
151 2005; <http://coulombstress.org>). Aside from the governing equations, the difference in
152 using linear vs. non-linear hydrodynamic models lies in the boundary conditions. The
153 linear model uses reflective boundary conditions and is therefore unable to perform
154 explicit run-up calculations at the shallow water areas along the coast. On the other
155 hand, the non-linear model uses moving boundary conditions and is capable of explicit
156 run-up calculations. The linear model was used in this study, because no attempt was
157 made to calculate run-up. The output files used for all interpretations are depth and

158 maximum wave amplitude files. The depth file contains the bathymetry of the region
159 where the simulation took place. An ETOPO2, 2551x1457 bathymetry grid with 2
160 arcmin resolution was used for all simulations. The maximum wave amplitude file
161 contains the calculated maximum sea level amplitude for a selected region, throughout
162 an entire simulation run (tsunami propagation time of 10-11.25 hours).

163

164 *3.2 Tsunami theory and numerical model limitations*

165 Tsunami theory has been studied by many authors. The following section sums up
166 tsunami theory based upon Liu et al (1998) and Ward (2002). The leading wave of a
167 tsunami has a wavelength proportional to the longitudinal dimensions of the earthquake
168 source region, which could be several hundreds to a thousand kilometers for a major
169 earthquake. It is considered to be a shallow water gravity wave, where the ocean depth is
170 negligible compared to the wavelength. Its phase speed is proportional to \sqrt{gh} , where, g
171 is the acceleration of gravity and h is the water depth in meters. The wave period ranges
172 between several hundreds to several thousand seconds. During propagation in deep water,
173 tsunami wave slope is small, resulting in insignificant convective inertia forces, which
174 can be ignored. As tsunamis propagate into the shallower water region, the wave
175 amplitude increases and the wavelength decreases due to shoaling. The nonlinear
176 convective inertia force becomes increasingly important. In the very shallow water, the
177 bottom frictional effects become significant as well. Therefore, the nonlinear shallow
178 water equations including bottom frictional terms should be used in the description of the
179 tsunami inundation. In principle, numerical computation of wave heights based on linear
180 shallow water equations is sufficient and accurate as long as the modeled tsunami
181 wavelength is much greater than water depth and the wave amplitude is much smaller
182 than water depth. This principle holds up until the deep part of the continental shelf.
183 Consequently, this study is unable to provide definite run-up results and only relative
184 amplitudes can be taken into consideration.

185 The time step chosen for each simulation must meet the Courant-Friedrichs-Lewy
186 (CFL) condition (Courant et al., 1928) in order to assure numerical stability. The CFL
187 condition for explicit numerical methods assures that the algorithm used for solving
188 partial differential equations is convergent. For the COMCOT modified explicit scheme,

189 the largest allowable Courant number is 0.8660 (Liu et al., 1998). Therefore, in order to
190 assure stability the time step used in this study never exceeded 3 seconds.

191

192 *3.3 Tsunami amplitude*

193 Two methods were used to reliably calculate wave amplitude. First, the amplitude
194 was calculated at depths of 250 m (see 'shelf point' in Fig. 3), similar to ten Brink et al.
195 (Chapter 7, 2007), in selected sites along the U.S. East Coast, the Caribbean Islands,
196 Europe, and Africa (Fig. 2). This depth falls within the minimal wavelength to grid size
197 ratio (see section 3.2 for detail), allowing for accurate propagation and amplitude
198 calculations. Second, a rectangular patch of different sizes (Fig. 3) was chosen seaward
199 of each location along the Atlantic, Caribbean, African and European coasts (Fig. 2).
200 The average amplitude was calculated for all of the points within the depth range of 150
201 to 50 m in each patch. The size of the patches varied depending on the geographical
202 locations where the amplitudes are measured. Along the U.S. East Coast for instance,
203 where the shelf is wide, larger patches were selected to account for as many points as
204 possible within the 150 to 50 m depth range. In the Caribbean, where the shelf is
205 narrower, smaller patches were sufficient to incorporate a representative number of
206 points in the same depth range. Although amplitudes calculated at such shallow depths
207 may be inaccurate in terms of their geographical locations, averaging them out over a
208 large area gives a good indication of the wave amplitude in that particular region. This
209 method also verifies that the amplitude calculated at a nearby shelf edge point of 250 m
210 depth is not anomalous. Figs. 4a and 4b show a comparison between amplitudes
211 calculated using the two methods, from an earthquake source located in location 8 (Fig.
212 3). Indeed, the average amplitudes calculated in the patches in the shallower water show
213 similar or higher amplitudes in comparison to the ones calculated in the slightly deeper
214 shelf edge points, as one would expect from the amplification effects of shallow waters.

215

216 *3.4 A method to overcome unreliable historical reports of run-up observations*

217 Caution must be exercised when using historical reports in order to compare between
218 possible epicenter locations. Table 1 shows the variability of run-up amplitudes in
219 historical reports, particularly in the Azores, Madeira, Lisbon and Tangier. It is therefore
220 impossible to compare our model results to individual run-up reports. Moreover, run-up

221 amplitudes are highly sensitive to the near shore bathymetry and onshore topography
 222 whereas, because of the model limitations discussed in sections 3.1 and 3.2, amplitudes
 223 were calculated at a water depth of 250 m. We therefore grouped together places in the
 224 Caribbean, along the Portuguese and Moroccan coast, in Madeira and the Azores, as
 225 locations representing consistent reports of high amplitudes. Earthquake sources
 226 generating high tsunami amplitudes in those locations are therefore assigned as a good fit
 227 to the 1755 Lisbon earthquake epicenter. Similarly, we joined together places along the
 228 U.S. East Coast and in Vigo and La Coruña in the northern Spanish coast, under a
 229 category of places where no historical reports were documented (i.e., negative evidence).
 230 Blank, (2008) quotes a French report from 1756 about a tsunami striking La Coruña, but
 231 the report itself does not mention tsunami there (Anonyme, 1756) , we interpret the
 232 general lack of reports from this established harbor to indicate that its amplitude was
 233 small. The particular locations along the U.S. East Coast (with the exception of Virginia
 234 Key in Florida), and Vigo and La Coruña in Spain, were chosen because they were
 235 already populated at the time of the earthquake yet there were still no tsunami reports
 236 found in the literature. In places along the U.S. East Coast, the tsunami should have
 237 struck during daylight hours. The semi-diurnal tidal ranges along the U.S. East Coast are
 238 <3 m and the difference between the times that high-tide reaches different locations along
 239 the East Coast is as large as 5 hours. Therefore, had a significant tsunami impacted the
 240 U.S. East Coast, some sites there would have experienced flooding during low tide. In
 241 NW Spain, both the time the tsunami should have struck and the tide conditions are
 242 similar to the other locations further south along the coast. Therefore, neither tidal
 243 variations nor time of the day are likely to explain the absence of reports in these
 244 locations. Table 2 summarizes the criteria used to group the historical reports.

245 In order to quantify the results we compared and normalized the amplitudes of all
 246 sources relative to source 5 (shown in Fig. 3). For each location j out of a total of n along
 247 the coasts (shown in Fig. 2 and Table 1) where no amplitudes were reported, we
 248 calculated the amplitudes of different model sources relative to that of source 5 using:

$$249 \quad Amp_i^{\min} = \sum_{j=1}^n (Amp_5 - Amp_j) / Amp_5 \quad (1)$$

250 where i represents the 16 model epicenter locations shown in Figure 3 . A better
 251 fitting epicenter location for any one of the examined model locations along the coasts

252 would generate wave amplitudes lower than that of source 5 and, thus, receive a positive
253 rating relative to source 5. Similarly, for each location k out of a total of m where high
254 amplitudes were reported (shown in Fig. 2 and Table 1), we calculated the amplitudes of
255 the sources relative to that of source 5 using

$$256 \quad Amp_i^{\max} = \sum_{j=1}^n (Amp_j - Amp_5) / Amp_5 \quad (2)$$

257 where i represents the 16 epicenter locations shown in Figure 3. A better fitting
258 epicenter location for any one of the locations along the coasts would generate wave
259 amplitudes higher than source 5 and, consequently, receive a positive rating relative to
260 source 5. As a result, the best fitting source i should maximize:

$$261 \quad [Amp_i^{\min} + Amp_i^{\max}] \quad (3)$$

262 Figures 5, 6, 7 and 17 were created using equations 1,2 and 3. Similar results were also
263 obtained when we excluded the Azores, Madeira and Lisbon, where there was a large
264 variation in the reported run-up amplitude, from the calculations.

265

266 **4. Results**

267 Fig. 3 and Table 3 show all the earthquake sources that were modeled. To facilitate a
268 meaningful comparison among the models, and for lack of detailed geologic constraints
269 for any of the sources, all the models used the same fault dip, dimensions, slip and
270 rigidity (Table 4) as those proposed for GBF (Johnston, 1996). Gorringe Bank is the most
271 prominent morphological feature in the area and was suggested to be capable of
272 generating an earthquake with a moment magnitude of 1.26×10^{22} Nm, similar to the one
273 calculated for the 1755 Lisbon earthquake (Johnston, 1996). The rigidity value used for
274 the moment magnitude calculation was very high (6.5×10^{10} Pa), to account for a fault that
275 is almost entirely within oceanic mantle lithosphere (Johnston, 1996). Furthermore, the
276 use of a pure thrust fault with rake 90° , would result in the highest possible transoceanic
277 tsunami amplitudes (see Geist, 1999), enabling us to test each individual feature that
278 govern tsunami propagation, separately.

279

280 *4.1 The effect of fault orientation on tsunami propagation and amplitudes*

281 The first set of simulations was designed to examine the effect of strike orientation on
282 tsunami propagation. Source 3 was chosen for this set because it is the one least
283 susceptible to near-source bathymetric effects in the fault region. The fault strike was

284 rotated 360° at 15° interval. Figure 8 shows the variations of maximum wave amplitude
285 as a function of fault orientation, for sites along the U.S. East Coast and the Caribbean. A
286 pattern of two maxima at fault strikes of 165°-180° and 345° yields the highest
287 amplitudes in the Caribbean. A fault strike of 345° is the equivalent to a thrust fault
288 dipping to the ENE (see dashed fault over source 3 in Figure 3) and was chosen as a
289 reference model. In this configuration, the leading westward propagating wave is a
290 depression phase (ocean withdrawal), followed by an elevation phase (flooding), in
291 agreement with observations from Madeira (Reid, 1914), Brazil (Kozak et al., 2005;
292 Ruffman, 2006), Newfoundland (Ruffman, 1990), and the Caribbean (O’Loughlin and
293 Lander, 2003). The minima are for fault strikes of 75°-90° and 270°-285°. Note that
294 GBF, which was suggested as a possible source for the 1755 Lisbon earthquake
295 (Johnston, 1996) has strike of 60°, close to one of the amplitude minima. Similarly, many
296 of the tectonic features proposed by Zitellini et al. (2004), which are oriented sub-parallel
297 to the Goringe Bank, would have also generated low tsunami amplitudes for the
298 Caribbean, contrary to observations.

299 Figure 6 compares fault orientations for source 5, one of our two preferred source
300 locations for the 1755 Lisbon earthquake. It shows that according to the criteria
301 developed in Section 3.4, source orientation of 345° fits better than source orientations of
302 330° and 360° and much better than a source oriented at 60°.

303

304 *4.2 The effect of different source locations on tsunami propagation and amplitudes*

305 A fault strike of 345° yields the highest amplitudes in the Caribbean in accordance
306 with historical reports and was therefore used when searching for fault location of the
307 1755 Lisbon earthquake (see section 4.3). Sixteen fault locations were modeled as
308 tsunami sources in the region of study (Fig. 3) and tsunami amplitudes were calculated in
309 locations along the U.S. East Coast and the Caribbean as well as along the European and
310 African coasts. Fault orientation for all locations was assumed to be 345° following the
311 analysis in Section 4.1. Figure 5 shows a comparison between the different source
312 locations relative to source 5. Based on the method outlined in Section 3.4, only source 8
313 fits better than source 5 and source 2 fits slightly worse. Note that source locations 8, 5,
314 and 2 are all located within the Horseshoe Plain. Figure 7 shows a comparison between
315 source 5, source 8 and the three previously suggested source locations GBF, MPF, and

316 GCF. It is clear that these three source locations are a poorer fit to the observations than
317 sources 5 and 8. Figures 9, 10 and 11 show maximum wave amplitude plots from
318 earthquake sources located in GBF, GCF and MBF respectively. Figures 9 and 10
319 highlight the same conclusion that is portrayed graphically in Figure 7. The maximum
320 wave amplitude generated from GBF (060°) is seen in a direction that is almost
321 perpendicular to that observed by the historical reports. As a result, the Caribbean Islands
322 are unaffected. Contrary to historical reports the wave amplitudes along the U.S. East
323 Coast, generated from GCF (349°) are high ($\sim 0.5\text{m}$) and spread over a relatively wide
324 area (as far north as Charleston). MPF from Figure 11 cannot be discounted, because it
325 shows that the U.S. East Coast remains relatively untouched and high wave amplitudes
326 are seen in the direction of the Caribbean, thus in agreement with historical reports.
327 Nevertheless, the results shown in Fig. 7 as well as comparing between MPF and sources
328 5 and 8 (Figs. 13, 14), indicate that MPF is less likely to be the 1755 Lisbon earthquake
329 source.

330

331 *4.3 The 1755 Lisbon earthquake epicenter and fault strike*

332 Figures 5 and 7 indicate that the most likely epicenter of the 1755 Lisbon earthquake
333 according to our model simulations is in the Horseshoe Plain area of sources 5 and 8 and
334 not in the previously suggested locations: GBF, MPF and GCF. The Horseshoe Plain
335 area is characterized by high seismicity and is cut by NE-SW trending thrust faults
336 which reach the seafloor (e.g., Sartori, 1994, Zitellini, 2004). Figures 6 and 8, however,
337 illustrate that the fault was most likely trending NW-SE as opposed to the previously
338 interpreted NE-SW strike orientation. The only known tectonic feature with a NW-SE
339 trend in this area is the inferred Paleo Iberia-Africa Boundary (PIAB), the equivalent
340 structure to the Newfoundland transform fault on the North American plate, which was
341 formed during the opening of the central Atlantic ocean in the Late-Jurassic-Early
342 Cretaceous (Rovere et al., 2004) (Fig. 1). However, further seismic and multibeam
343 investigations of the west Horseshoe Plain are necessary to test if the PIAB is currently
344 active.

345

346

347

348 *4.4 Near field tsunami travel times*

349 Constraining source location based on tsunami travel time is problematic (Gutscher et al.,
350 2006) due to the inaccuracy of historical reports (e.g., a 30 minute difference in arrival
351 time between Porto Santo and Madeira Islands which are only 50 km apart), due to the
352 possibility of landslide-generated tsunamis, and due to the difficulties in simulating
353 tsunami propagation at shallow depths (see section 3.2)

354 Nevertheless, we computed travel times to locations of historical reports assuming simple
355 aerial distance, tsunami phase speed of \sqrt{gh} with water depths ranging from 2500 m to
356 4500 m for sources 5 and 8 and 1000 m to 4000 m from source 2 (Table 5), Travel times
357 from historical reports were listed by Baptista et al. (1998a) and Gutscher et al. (2006).
358 Although source location 2 (near MPF) seems to be the best with respect to some of the
359 historical reports, the overall time differences between source location 2 and sources 5
360 and 8 is minor, implying that an epicenter located further to the west is not unlikely.

361

362 **5. Discussion**

363 *5.1 The effects of regional and near-source bathymetry on tsunami propagation and*
364 *amplitude*

365 Regional and near-source bathymetry have a significant effect on tsunami
366 propagation in the Atlantic. In a hypothetical case lacking bathymetric features, a tsunami
367 is expected to propagate uniformly in all directions along great circle paths. Figure 12
368 shows a plot of maximum wave amplitude across the Atlantic ocean from source 5. The
369 black lines indicate great circles from earthquake source 5 to different locations along the
370 U.S. East Coast and the Caribbean. The trace of relatively high wave amplitudes in the
371 direction of Virginia Key in southern Florida represents the only wave packet closely
372 following a great circle. All other wave amplitude traces relevant to the locations along
373 the U.S. East Coast and the Caribbean suggest that the corresponding wave packets were
374 either dispersed or deflected by various bathymetric features. Figures 13 and 14 show a
375 maximum wave amplitude plot from sources 8 and 5 focusing on far-field and near-
376 source effects, respectively. Figure 14 suggests that the wave propagating eastward
377 toward the Portuguese coast is unaffected by deep ocean bathymetry, whereas Figure 13
378 implies that propagation westward has a fingering pattern due to wave scattering by
379 bathymetry. The near-source bathymetric elements causing such scattering are the

380 Gorringe Bank, the Ampere and Coral Patch seamounts as well as Madeira Island and the
381 MTR. These bathymetric elements are much shallower than 1500 m, which is the
382 minimal depth required to scatter a tsunami wave according to the analytical analysis of
383 Mofjeld et al. (2000). The energy is first highly influenced by the Ampere and Coral
384 Patch seamounts as well as the MTR and Madeira Island. Farther to the west, wave
385 propagation seems to be influenced by the Mid-Atlantic ridge; in particular the Azores
386 and the Great Meteor and Cruiser seamounts. Higher amplitudes are shown in the vicinity
387 of these bathymetric elements. However, the wave amplitudes decay quickly behind these
388 bathymetric features because these features tend to attenuate the low frequency waves.
389 On the other hand, tsunami wave energy is inferred to be traversing through the low part
390 of the MTR (arrow in Fig. 14) and later in between the Azores and Great Meteor and
391 Cruiser seamounts, following a great circle toward southern Florida; this wave phase
392 maintains its low frequency content and reaches its trans-Atlantic destination with much
393 higher amplitude. We believe the reason why there are no reports from the 1755 tsunami
394 in southern Florida could be attributed to the northern Bahamas Banks (NBB) which may
395 have acted as a barrier to that area. The rest of the U.S. East Coast remains relatively
396 protected. The northern part of the MTR may have played an important role in shielding
397 the United States, scattering wave energy in that direction. Similarly, the Coral Patch and
398 Ampere seamounts as well as Madeira Island seem to partially scatter the energy in the
399 direction of the Caribbean. The same energy is later scattered a bit more by the Great
400 Meteor and Cruiser seamounts. It is possible that the trace of relatively high amplitudes
401 southward of the Great Meteor seamount may correspond to refracted tsunami energy,
402 responsible for run-up reports in Brazil (Kozak et al., 2005; Ruffman, 2006). Scattering
403 energy by seamounts, however, is relatively ineffective (Mofjeld et al., 2000), allowing
404 enough energy to reach the Caribbean, thus explaining the historical reports. Additional
405 simulations using high-resolution near-shore bathymetry could verify the historical
406 reports claiming that some islands in the Caribbean have experienced greater run-ups
407 than others. Historical run-up reports exist for the entire Antilles arc beginning in
408 Santiago de Cuba and ending in Barbados with the exception of San Juan, Puerto Rico. A
409 possible explanation for the absence of a tsunami report from San Juan is the presence of
410 the ultra-deep Puerto Rico trench (-8350 m) north of San Juan, which may have deflected
411 the energy of the ray path that arrived in a sub-critical angle. (Mofjeld et. al, 2000; Mei,

412 1999). The waves propagating northward (as indicated from the high wave amplitudes),
413 amid the Gorringe Bank and the Josephine seamount and then passing north of the
414 Azores, may have eventually reached Newfoundland, Canada, explaining the historical
415 reports there. Finally, the wave energy that passed southward east of the Coral Patch
416 seamount may explain the historical reports in the Canary Islands (Reid, 1914).

417

418 *5.2 Implications to tsunami hazard to the U.S. East Coast*

419 The effect of near-source bathymetry on tsunami propagation was tested in order to
420 assess tsunami hazard to the U.S. East Coast from possible future earthquakes in the
421 study area. Two sources were compared: one east and one west of the MTR because both
422 regions have the potential to generate sufficiently strong earthquakes (Buforn et al.,
423 1988). For both sources the maximum wave amplitude was calculated for fault strike
424 orientations varying from 0-360° at 15° interval as described in section 4.1. The wave
425 amplitudes were then averaged out over 360° and measured at deep water locations 3500
426 and 4000 km (shown by stars in Fig. 2) from sources 16 and 3, respectively. These deep
427 water locations lie along the azimuths of the U.S. East Coast and the Caribbean coastal
428 sites. A 10% amplitude reduction was factored in to compensate for the difference in
429 distance between 3500 and 4000 km (Ward, 2002) in order to properly compare between
430 the two sources (Fig. 15). If bathymetry had no effect on wave propagation one would
431 expect wave amplitudes to be identical. The fact that amplitudes vary, further
432 demonstrates the significant effect of the bathymetry on transatlantic tsunami
433 propagation. The calculations from source 3 illustrate an amplitude distribution pattern
434 very similar to that depicted in Figures 10 with a maximum in the direction of Virginia
435 Key.). Wave amplitudes from an earthquake source west of the MTR (source 16) show
436 an entirely different amplitude distribution pattern, revealing higher amplitudes in the
437 direction of Baltimore and southward down to Cape Hatteras (Azimuth 292 from source),
438 signifying possible tsunami hazard to these regions. All other places calculated from
439 source 16 show a decrease in amplitudes, except for the waves heading towards
440 Charleston, while the amplitude for Dominica remains relatively unchanged. Figure 16
441 shows a maximum wave amplitude plot from source 16, for a fault with a strike of 30°,
442 west of and adjacent to the MTR. This plot may suggest a possible greater hazard to the
443 U.S. East Coast from earthquakes located in the region west of MTR. We should note,

444 however, that the region west of MTR has so far generated only strike-slip earthquakes
445 (Grimison and Chen, 1986; Buform et al., 1988) and relative motion there is predicted by
446 plate kinematic models to be strike-slip (Argus et al., 1989; Nocquet and Calais, 2004).
447 Figure 17 compares all the different earthquake sources relative to source 5 with respect
448 to the U.S. East Coast only (excluding the Virginia Key), in the same way described in
449 section 3.4. In all cases the fault strike was 345° , because it yields the highest amplitudes
450 in the direction of the United States, as shown in Figure 8. Source locations 3 and 1 in the
451 Gulf of Cádiz and locations west and north of the Gorringe Bank are calculated to
452 generate the highest amplitude tsunamis along the U.S. East Coast, highlighting the
453 potential hazard from these sources. Figure 10 further demonstrates the potential tsunami
454 hazard to the U.S. East Coast from earthquake sources located in the Gulf of Cádiz.
455 Figure 11, on the other hand, shows low tsunami risk from an earthquake source located
456 in the MPF. We can therefore conclude that the Gorringe Bank and the north MTR may
457 protect the U.S. East Coast from earthquakes in the Horseshoe Plain, the MPF, the SVF
458 and their surrounding area, but not from the Gulf of Cádiz. Finally, it is important to note
459 that only thrust earthquakes, roughly striking northward may pose tsunami hazard to the
460 U.S. East Coast.

461

462 *5.3 Other considerations – shelf width*

463 The continental shelf along the U.S. East Coast is much wider than along the
464 Caribbean Islands. The large shelf width may have contributed to the dissipation of
465 tsunami amplitude along the U.S. East Coast and is perhaps one reason for the lack of
466 historical reports from the 1755 Lisbon tsunami. Due to the limitations imposed by the
467 low-resolution bathymetry (section 3.2), we were unable to quantitatively calculate the
468 shelf width effect on wave amplitudes. Nevertheless, Figs. 12 and 13 illustrate that
469 amplitudes in southern Florida are higher than in other areas along the East Coast
470 although the continental shelf in Florida is wider. This suggests that shelf width affects
471 tsunami propagation and amplitudes less than the source fault strike orientation and the
472 seafloor bathymetry along the wave paths.

473

474 **6. Conclusions**

475 Methodological tsunami simulations based upon historical reports of both far field
476 and near field effects of the November 1st, 1755 Lisbon tsunami suggest three important

477 conclusions: First, the earthquake seems to have been generated by a NW-SE trending
478 fault located in the center of the Horseshoe Plain, south of the Gorringe Bank. This
479 orientation is almost perpendicular to previously suggested NE-SW trending faults such
480 as GBF and structures south of the Gorringe Bank (Zitellini, 2001). The only known
481 tectonic structure with a NW-SE orientation in this area is the PIAB, although its
482 potential for reactivation remains ambiguous. Moreover, the modeling results allow us to
483 discount the GCF and to a lesser extent the MPF, because both are located too far to the
484 east of the Horseshoe Plain. The GCF can be discounted as a tsunami source because it
485 is predicted to generate relatively high wave amplitudes along the U.S. East Coast, and
486 relatively low ones along the Caribbean. The orientation and location of the MPF are
487 slightly less favorable than our preferred sources in the Horseshoe Plain, even when
488 considering historical reports of tsunami arrival times.

489 Second, seafloor bathymetry is a significant factor in dictating transatlantic tsunami
490 propagation. In particular, the bathymetry of the Gorringe Bank, the MTR (Josephine
491 Seamount) and the Azores allows waves to reach Newfoundland, but blocks them from
492 reaching most of the U.S. East Coast, with the exception of southern Florida. The
493 Ampere and Coral Patch seamounts, Madeira Island, and the Great Meteor and Cruiser
494 seamounts reduce wave propagation toward the Caribbean. The latter two features
495 partially refract wave energy toward Brazil. Furthermore, high run-up reports in the
496 Caribbean are most likely due to the steep rise in the bathymetry near to shore.

497 The third conclusion concerns tsunami hazards to the U.S. East Coast from sources
498 located along the eastern Iberian-African plate boundary, which generate sufficiently
499 strong thrust earthquakes. The Gorringe Bank and the north MTR act as near source
500 barriers, protecting most of the U.S. East Coast. For sources located east of MTR and
501 south of the Gorringe Bank, Florida might be at risk if sufficient wave energy manages to
502 pass through the Bahamas. Sources in the Gulf of Cádiz may present a wider hazard to
503 the U.S. East Coast, because they are sufficiently south as to not be affected by the
504 Gorringe Bank, north MTR, and the Azores. For sources located west of the MTR, the
505 risk is shifted northward in the direction of Baltimore.

506 It is important to note that the interpretations in this report considered relative
507 amplitudes only. High resolution near-shore bathymetry is crucial for more accurate run-
508 up calculations and tsunami hazard assessments.

509

510 **Acknowledgments**

511 Propagation models were obtained using the Cornell Multi-grid Coupled Tsunami Model
512 (developed by Liu et al., 1998) in the Tsunami Computational Portal; the Portal is a joint
513 project of the Northwest Alliance for Computational Science & Engineering at Oregon
514 State University (www.nacse.org) and the Arctic Region Supercomputing Center
515 (www.arsc.edu) at the University of Alaska-Fairbanks. We thank Dylan Keon and Harry
516 Yeh (Oregon State University) and Tom Logan and Elena Suleimani (Arctic Region
517 Supercomputing Center) for assistance with running the models. We would further like to
518 thank Xiaoming Wang (Cornell University) for technical consultations and assistance,
519 Eric Geist (U.S. Geological Survey, Menlo Park) for fruitful discussions, and Hyun-Sook
520 Kim, Jason Chaytor, and Brian Andrews (U.S. Geological Survey, Woods Hole) for
521 technical assistance. Helpful reviews by Eric Geist and Alberto Lopez, two anonymous
522 reviewers, and Editor David Piper are gratefully acknowledged. Roy Barkan thanks the
523 Woods Hole Oceanographic Institution Summer Student Fellowship Program for their
524 financial support and hospitality. Roy Barkan would further like to thank Shmulik Marco
525 (Tel Aviv University) for providing the technical means to complete this study. This
526 study was funded by the U.S. Nuclear Regulatory Commission under NRC Job Number
527 N6408 *Physical study of tsunami sources*.

528

529 **References**

- 530 Anonyme, (1756). J. Historique sur les Matie'res du Tems (T. 79) Jan. 1756, 41-45
531 (<http://gallica.bnf.fr/ark:/12148/bpt6k105284f/f2.table>).
- 532 Argus, D.F., Gordon, R.G., DeMets, C., Stein, S., 1989. Closure of the Africa-Eurasia-
533 North America plate motion circuit and tectonics of the Gloria fault. J. Geophys. Res.
534 94, 5585-5602.
- 535 Baptista, M.A., Heitor, S., Miranda, J.M., Miranda, P.M.A., Mendes Victor, L., 1998a.
536 The 1755 Lisbon earthquake; evaluation of the tsunami parameters. J. Geodyn. 25,
537 143–157.
- 538 Baptista M.A., Miranda, P.M.A., Miranda, J.M., Mendes Victor, L., 1998b. Constraints
539 on the source of the 1755 Lisbon tsunami inferred from numerical modeling of
540 historical data on the source of the 1755 Lisbon tsunami. J. Geodyn. 25, 159–174.

541 Baptista, M.A., Miranda, J.M., Chierici, F., Zitellini, N., 2003. New study of the 1755
542 earthquake source based on multi-channel seismic survey data and tsunami modeling.
543 Nat. Hazards Earth Sci. Syst. 3, 333–340.

544 Baptista, M.A., Miranda, J.M., Luis, J.F., 2006. In search of the 31 March 1761
545 earthquake and tsunami sources, Bull. Seismol. Soc. Am., 96, 713-721.

546 Blank, P.L., 2008. The tsunami in Cadiz on 1 November 1755: A critical analysis of
547 reports by Antonio Ulloa and Louis Godin, CRAS2A-2718, 11 pp.

548 Borges, J.F., Fitas, A. J. S., Bezzeghoud, M., and Teves-Costa, P., 2001. Seismotectonics
549 of Portugal and its adjacent Atlantic area, Tectonophys., Vol. 337, 373-387.

550 Buforn E., Udías, A., Mézcua, J., 1988. Seismicity and focal mechanisms in south Spain.
551 Bull. Seism. Soc. Am. 78, 2008-2224.

552 Buforn E., M. Bezzegoud, A. Udias, C. Pro, 2004. Seismic Sources on the Iberia-African
553 Plate Boundary and their Tectonic Implications. Pure and Appl. Geophys., 161, 623-
554 626

555 Chester, D.K., 2001. The 1755 Lisbon earthquake. Prog. Phys. Geogr. 25, 363–383.

556 Courant R., Friedrichs, K., Lewy, H., 1928. Über die partiellen Differenzgleichungen
557 der mathematischen Physik. Mathematische Annalen. 100 (1), 32–74.

558 Fernandes R.M.S, Miranda J.M., Meijninger B.M.L., Bos M.S., Noomen R., Bastos L.,
559 Ambrosius B.A.C., Riva R.E.M., 2007. Surface Velocity Field Of The Ibero-
560 Maghrebian Segment Of The Eurasia-Nubia Plate Boundary. Geophys. J.
561 Int. 169 (1), 315-324.

562 Fukao, Y., 1973. Thrust faulting at a lithospheric plate boundary: The Portugal
563 earthquake of 1969. Earth Planet. Sci. Lett., 18, 205-216.

564 Geist, E.L., 1999. Local tsunamis and earthquake source parameters. Adv. Geophysics,
565 39, 117-209.

566 Gisler, G., Weaver, R., Gittings, M. L., 2006. SAGE calculations of the tsunami threat
567 from La Palma. Science of Tsunami Hazards, 24, 288-301.

568 Grácia, E., Danõbeitia, J.J., Vergés, J., PARSIFAL team, 2003a. Mapping active faults
569 offshore Portugal (36°N–38°N): Implications for seismic hazard assessment along the
570 southwest Iberian margin. Geology. 31, 83– 86.

571 Grácia, E., Pallas, R., Casas, D., Willmot, V., Grácia -Orellan, J., Danõbeitia, J.J., The
572 Hits Cruise Party, 2003b. Submarine landslides associated to active faulting offshore

573 Portugal (SW Iberian Margin): Paleoseismic implications. EGS–AGU–EUG Joint
574 Assembly, Abstracts from the meeting held in Nice, France, 6–11 April 2003, abstract
575 #13064.

576 Grandin, R., Borges, J.F., Bezzeghoud, M., Caldeira, B., Carrilho, F., 2007. Simulations
577 of strong ground motion in SW Iberia for the 1969 February 28 ($M_s=8.0$) and the
578 1755 November 1 ($M \sim 8.5$) earthquakes – I. Velocity model. II. Strong ground
579 motion simulations. *Geophys. J. Int.* 171(2), 807-822(16).

580 Grimison, N.L., and Chen, W., 1986. The Azores-Gibraltar plate boundary: Focal
581 mechanisms, depth of earthquakes and their tectonical implications. *J. Geophys. Res.*
582 91, 2029-2047.

583 Gutscher, M.A., Malod, J., Rehault, J.P., Contrucci, I., Klingelhoefer, F., Mendes-Victor,
584 L., Spackman, W., 2002. Evidence for active subduction beneath Gibraltar. *Geology.*
585 30, 1071- 1074.

586 Gutscher, M.-A., 2004. What caused the Great Lisbon earthquake? *Science.* 305, 1247–
587 1248.

588 Gutscher, M.-A., Baptista, M.A., Miranda, J.M., 2006. The Gibraltar Arc seismogenic
589 zone: Part 2. Constraints on a shallow east dipping fault plane source for the 1755
590 Lisbon earthquake provided by tsunami modeling and seismic intensity.
591 *Tectonophysics.* 426,153-166.

592 Hayward, N., Watts, A.B., Westbrook, G.K., Collier, J.S., 1999. A seismic reflection and
593 GLORIA study of compressional deformation in the Goringe Bank region, eastern
594 North Atlantic. *Geophys. J. Int.* 138, 831-850.

595 Johnston, A., 1996. Seismic moment assessment of earthquakes in stable continental
596 regions –III New Madrid 1811-1812, Charleston 1886 and Lisbon 1755. *Geophys. J.*
597 *Int.* 126, 314-344.

598 Kozak, J.T., Moreira, V.S., Oldroyd, D.R., 2005. Iconography of the 1755 Lisbon
599 Earthquake. Academy of Sciences of the Czech Republic, Prague, 82 pp.

600 Lin, J., Stein, R.S., 2004. Stress triggering in thrust and subduction earthquakes, and
601 stress interaction between the southern San Andreas and nearby thrust and strike-slip
602 faults. *J. Geophys. Res.* 109, B02303, doi:10.1029/2003JB002607.

603 Liu, P.L.-F., Woo, S.-B., and Cho, Y.-S., 1998. Computer Program for Tsunami
604 Propagation and Inundation, sponsored by National Science Foundation.
605 http://ceeserver.cce.cornell.edu/pll-group/comcot_down.htm.

606 Lockridge, P.A., Lowell, S., Whiteside, L.A., Lander, J.F., 2002. Tsunamis and tsunami-
607 like waves of the Eastern United States. *Int. J. Tsunami Soc.*, 20(3), 120-157.

608 Machado, F., 1966. Contribução para o estudo do terremoto de 1 de Novembro de 1755.
609 *Rev. Fac. Ciên. De Lisbon. Ser. C*, 14, 19-31.

610 Mader, C.L., 2001. Modeling the 1755 Lisbon tsunami. *Science of Tsunami Hazards*. 19,
611 93-116.

612 Martinez-Solares, J.M., Lopez, A., Mezcuca, J., 1979. Isoleismal map of the 1755 Lisbon
613 earthquake obtained from Spanish data. *Tectonophysics*, 53, 301-313.

614 Mei, C. C., 1989. *The Applied Dynamics of Ocean Surface Waves*. World Scientific,
615 Section 3, pp. 740, Singapore.

616 Mofjeld, H.O., Titov, V.V., Gonzalez, F.I., Newman, J.C., 2000. Analytic Theory of
617 Tsunami Wave Scattering in the Open Ocean With Application to the North Pacific,
618 NOAA Technical Memorandum OAR PMEL-116.

619 Moreira, V.S., 1985. Seismotectonics of Portugal and its adjacent area in the Atlantic.
620 *Tectonophysics*. 117, 85-96.

621 Nocquet, J.M., Calais, E., 2004. Geodetic measurements of crustal deformation in the
622 Western Mediterranean and Europe. *Pure Appl. Geophys.* (161), 661-681.

623 O'Loughlin, K.F., Lander, J.F., 2003. Caribbean tsunamis: A 500-year history from
624 1498-1998, Kluwer Academic Pub., 280 pp.

625 Reid, H.F., 1914. The Lisbon earthquake of November 1, 1755. *Bull. Seism. Soc. Am.*
626 4(2), 53- 80.

627 Rovere, M., Ranero, C.R., Sartori, R., Torelli, L., Zitellini, N., 2004. Seismic images and
628 magnetic signature of the Late Jurassic to Early Cretaceous Africa-Eurasia plate
629 boundary off SW Iberia. *Geophys. J. Int.* 158(2), 554–568.

630 Ruff, L.J., (2003). Some aspects of energy balance and tsunami generation by
631 earthquakes and landslides, *Pure Appl. Geophys.*, 160, 2155-2176.

632 Ruffman, A., 1990. Tsunamis of Eastern Canada, 1755- Present (Abstract). Workshop
633 JW.1. Tsunami Sources Around Europe, European Geophysical Society, XV General

634 Assemble, April 23-27, Copenhagen, Denmark. *Annales Geophysicæ*, Special issue.
635 Abstract JW.1-11, 334-335.

636 Ruffman, A., 2006. From an Ephemerides to 'Observation on The Changes of The Air':
637 Documenting The far-field parameters of the November 1, 1755 "Lisbon" Tsunami in
638 the western Atlantic (Abstract). Atlantic Geoscience Society 32nd Colloquium and
639 Annual Meeting, February 3-4, Greenwich, Nova Scotia. Program with Abstracts,
640 63-64. *Atlantic Geology*. 42(1), 111.

641 35. Sartori, R., Torelli, L., Zitellini, N., Peis, D., Lodolo, E., 1994. Eastern segment of
642 the Azores Gibraltar line (central-eastern Atlantic): An oceanic plate boundary with
643 diffuse compressional deformation. *Geology*. 22, 555–558.

644 Ten Brink, U., Twichell, D., Geist, E., Chaytor, J., Locat, J., Lee, H., Buczkowski, B.,
645 and Sansoucy, M., 2007. The current state of knowledge regarding potential tsunami
646 sources affecting U.S. Atlantic and Gulf Coasts, U.S. Geological Survey
647 Administrative Report, pp. 162.

648 Terrinha, P., Pinheiro, L.M., Henriët, J.-P., Matias, L., Ivanov, M.K., Monteiro, J.H.,
649 Akhmetzhanov, A., Volkonskaya A., Cunha, T., Shaskin, P., Rovere, M., 2003.
650 Tsunamigenic-seismogenic structures, neotectonics, sedimentary processes and slope
651 instability on the southwest Portuguese Margin. *Mar. Geol.* 195, 55-73.

652 Thiebot, E., Gutscher, M.A., 2006. The Gibraltar Arc seismogenic zone (part 1):
653 Constraints on a shallow east dipping fault plane source of the 1755 Lisbon
654 earthquake provided by seismic data, gravity and thermal modeling. *Tectonophys.*,
655 v.426(in press). 1-2, p.135-152. *Tectonophysics*, v.426(in press). 1-2, p.135-152.

656 Toda, S., Stein, R.S., Richards-Dinger, K., Bozkurt, S., 2005. Forecasting the
657 evolution of seismicity in southern California: Animations built on earthquake stress
658 transfer. *J. Geophys. Res.* B05S16, doi:10.1029/2004JB003415.

659 Ward, S.N., 2002. Tsunamis. *Encyclopedia of Physical Science and Technology*-
660 Academic Press. 17, 175-191. http://es.ucsc.edu/~ward/papers/tsunami_ency.pdf

661 Zitellini, N., Mendes-Victor, L., Córdoba, D., Dañobeitia, J., Nicolich, R., Pellis, G.,
662 Ribeiro, A., Sartori, R., Torelli, L., Bartolomé, R., Bortoluzzi, G., Calafato, A.,
663 Carrilho, F., Casoni, L., Chierici, F., Corela, C., Correggiari, A., Della Vedova, B.,
664 Gràcia, E., Jornet, P., Landuzzi, M., Ligi, M., Magagnoli, A., Marozzi, G., Matias,
665 L.M., Penitenti, D., Rodriguez, P., Rovere, M., Terrinha, P., Vigliotti, L., Zahinos

666 Ruiz, A., 2001. Source of the 1755 Lisbon earthquake and tsunami investigated. EOS
667 Trans. Amer. Geophys. U. 82, 285.
668 Zitellini, N., Rovere, M., Terrinha, P., Chierici, F., Matias, L., BIGSETS team, 2004.
669 Neogene through Quaternary tectonic reactivation of SW Iberian passive margin.
670 Pure Appl. Geophys. 161, 565– 587.

671

672

673

674 **Figure Captions**

675 Fig. 1. Plate tectonic setting (inset) and bathymetric map of the Iberian-African plate
676 boundary. Depth contours: Blue – 250 m; black – 1000, 1500, and 2000 m.

677 Barbed lines - proposed faults by previous studies: GBF - Gorringe Bank Fault; MPF -
678 Marqués de Pombal Fault; SVF- St. Vincente Fault; HSF - Horseshoe Fault; GCF - Gulf
679 of Cádiz Fault. PIAB refers to the Paleo Iberia- Africa Plate Boundary (Rovere et al.,
680 2004). Plates in inset: NAM – North America; EUR- Eurasia; AFR- Africa (after Grácia
681 et al., 2003a).

682

683 Fig. 2. Locations of run-up reports in Table 1 (red circles) except for Itamaraca and
684 Tamandare (located in Brazil). Also shown are locations along the U.S. East Coast and
685 Spain with no historical reports (open red circles).

686 Rectangles represent patches used to calculate average tsunami amplitudes on the shelf
687 (see section 3.3 for explanation).

688 Stars indicate points where average amplitudes over 360 degrees were measured (see
689 section 5.2 for explanation).

690

691 Fig. 3. Bathymetric map of the Iberian margin. Contours- same as Fig. 1. Epicenter
692 (placed in the center of finite fault) used to generate tsunami simulations are shown in
693 green circles with corresponding fault model number (see Table 3 for source
694 coordinates). Fault orientation for sources 3 and 16 were rotated 360° at 15° interval to
695 test for the optimal strike angle generating maximum amplitudes in the Caribbean (see
696 section 4.1 for explanation) to assess the tsunami hazard to the U.S. East coast (see
697 section 5.2 for explanation). Blue circles along the 250 m contour line represent the *shelf*
698 *points* where the tsunami amplitude was calculated seaward of each historical location.

699 Rectangles- same as in Fig. 2. Red circles represent cities with historical tsunami reports
700 (see Table 1).

701

702 Fig. 4. Comparison between absolute tsunami amplitudes for fault source location 8
703 measured at the shelf edge points at 250 m depth and averaged over rectangular patches
704 at depths of 50-150 m (see section 3.3 for explanation) for the Caribbean side (a) and for
705 the European and African side (b).

706

707 Fig. 5. Comparison between all fault sources shown in Fig. 3 and listed in Table 3. All of
708 the faults have strike of 345° and their other parameters are listed in Table 4. Positive
709 bars represent sources that are better fitting than source 5 to be the 1755 Lisbon epicenter.
710 Negative bars represent sources that are worse fitting than source 5 to be the 1755 Lisbon
711 epicenter (see section 3.4 for explanation). According to this test source 8 is the best
712 candidate source for the 1755 Lisbon earthquake.

713

714 Fig. 6. Comparison between tsunami amplitude from different fault orientations located
715 in source 5. Negative bars represent fault orientations that do not fit as well as the model
716 with strike of 345° (see section 3.4 for explanation). A strike of 60° , like the one
717 suggested for GBF, has the worst fitting.

718

719 Fig. 7. Comparison between sources 5 and 8 and the previously suggested sources of the
720 1755 Lisbon earthquake: GBF (Johnston, 1996); MPF (Zitellini et al., 2001); and GCF
721 (Gutscher et al., 2006) (sources 7, 4 and 1 respectively); fault strikes were 060° , 020° and
722 349° , respectively. Positive bars represent source locations that are better fitting than
723 source 5 to be the 1755 Lisbon epicenter. Negative bars represent source locations that
724 are less fitting than source 5 to be the 1755 Lisbon epicenter (see section 3.4 for
725 explanation). Both Sources 5 and 8 are better fitting than the three previously suggested
726 fault models.

727

728 Fig. 8. Comparison between the absolute tsunami amplitudes as a function of variation in
729 the fault strike orientation, using source 3. Maxima are at 165° - 185° and 345° and
730 minima are at 75° - 90° and 270° - 285° .

731

732 Fig. 9. Maximum wave amplitude from an earthquake source located in GBF. The strike
733 angle used is 60° similar to that suggested by Johnston (1996) and Grandin et al. (2007).
734 The scale ranges from 0-2 m, with 0.1 m intervals. The main wave energy propagates
735 NNW, leaving the Caribbean Islands almost unaffected.

736

737 Fig. 10. Maximum wave amplitude from an earthquake source located in GCF with fault
738 strike of 349° similar to that suggested by Gutscher et al. (2002; 2006) and Thiebot and
739 Gutscher (2006). Scale- same as in Fig. 9. Contrary to historical records low amplitudes
740 are seen in the vicinity of the Caribbean, whereas high amplitudes are seen along the U.S.
741 East Coast, south of Charleston.

742

743 Fig. 11. Maximum wave amplitude from an earthquake source located in MPF with fault
744 strike of 20° . Location and strike are after Zitellini et al. (2001) and Grácia et al. (2003a).
745 Scale- same as in Fig. 9. Note that although a tsunami generated at the MPF is not
746 expected to affect the U.S. Atlantic coast, it predicts lower amplitude in the Caribbean
747 and higher amplitude in northwest Spain than Fig. 13.

748

749 Fig. 12. Maximum wave amplitude projected on a sphere from an earthquake source
750 located in source 5. The scale ranges from 0-1 m. Warm colors indicate high amplitudes
751 and cold colors low amplitudes. Black lines indicate great circle paths between source 5
752 and locations along the U.S. East Coast and the Caribbean. The wave energy heading
753 toward Virginia Key in southern Florida is the only one following a great circle path. All
754 other wave energies are scattered by topography.

755

756 Fig. 13. Maximum wave amplitude from the best fit earthquake source located in source
757 8. Scale- same as in Fig. 9. Wave scattering is mainly caused by the Madeira Island,
758 Madeira Tore-Rise (MTR), the Azores, the Great Meteor (GM) and Cruiser (Cr)
759 seamounts. The ray passing in between the Azores and the Great Meteor seamount
760 reaches southern Florida. The rest of the U.S. East Coast is relatively unaffected by the
761 tsunami. NBB-northern Bahama Banks.

762

763 Fig. 14. Maximum wave amplitude from an earthquake source located in source 5,
764 illustrating the effects of near-source topography. The scale ranges from 0-5 m, with 0.1
765 m intervals. Tsunami propagation eastward is undisturbed by topography. High
766 amplitudes in the Goringe Bank, Coral Patch (CP) and Ampere (Amp) seamounts, and
767 Madeira Tore-Rise (MTR) are due to wave amplification by these relatively shallow
768 features (> -1500 m), although these features scatter the long period component (see
769 section 5.1 for explanation). The arrows represent a less-attenuated wave, which traverses
770 between the Azores and the Great Meteor seamount heading toward southern Florida (see
771 Fig. 13). Jos. Smt.- Josephine seamount.

772

773 Fig. 15. Comparison of tsunami amplitudes from sources located to the east (source 3)
774 and the west (source 16) of the MTR. Amplitudes are measured in deep water 4000 km
775 west from source 3 and 3500 km west from source 16 (see stars in Fig. 2). The
776 amplitudes are measured in the direction of sites along the U.S. East Coast and the
777 Caribbean as indicated at the bottom of each bar. Amplitudes from source 16 were
778 reduced by 10% in order to compensate for the 500 km shorter propagation path relative
779 to source 3 (Ward, 2002). Amplitudes were averaged over 24 fault orientations covering
780 360° at 15° interval. Differences in amplitudes illustrate the effect of the bathymetry on
781 tsunami propagation, in particular the effects of the north MTR.

782

783 Fig. 16. Maximum wave amplitude from an earthquake source located in source 16 and
784 oriented 30° . Scale- same as Fig. 9. High amplitudes are seen in a wider area along the
785 U.S. East Coast relative to Fig. 13, highlighting the greater hazard from earthquake
786 sources located west of MTR.

787

788 Fig. 17. Comparison between all of the modeled sources relative to source 5, for sites
789 along the U.S. East Coast (see section 3.4 for explanation). See Figure 3 and Table 3 for
790 source locations. Positive bars represent sources that may have a lower impact than
791 source 5 on the U.S. East Coast. Negative bars represent sources that are calculated to
792 have greater impact than source 5 to the U.S. East Coast (see section 5.2). Sources 1, 3,
793 12, 16 and 10 are calculated to have the greatest impacts to the U.S. East Coast.

794

Table 1

[Click here to download Table: Table 1.doc](#)

Table 1- Sites of historical tsunami runup reports, sites that were populated in 1755 but did not mention tsunami impact and sites with tsunami reports but no run-up reports

Location	Latitude (°N)	Longitude (°E)	Run-up (m)	Reference
Santiago de Cuba	20.010	-75.810	NRR	OL
Samaná Bay	19.139	-69.355	NRR	OL
St. Martin	18.060	-63.050	4.5	OL
Saba	17.630	-63.230	?-7	OL, Ba2, Ru
Antigua	17.090	-61.800	3.6	OL
Dominica	15.300	-61.380	3.6	OL
Barbados	13.250	-59.530	1.5-1.8	OL,Ba2
Itamaraca (Brazil)	-7.747	-34.825	NRR	Ru
Tamandare (Brazil)	-8.760	35.105	NRR	Ru
Bonavista	49.000	-53.333	NRR	Ru ,Re
Boston	42.358	-71.060	NR	
Baltimore	39.286	-76.615	NR	
New York	40.716	-74.000	NR	
Charleston	32.783	-79.933	NR	
Virginia Key	25.787	-80.216	NR	
Cornwall	50.130	-5.425	2-3.7	Ba2
La Coruña	43.366	-8.383	NR	
Vigo	42.237	-8.721	NR	
Porto	41.150	-8.633	1	Ba
Figueira	40.140	-8.880	NRR	Ba
Porto Novo	39.100	-9.430	NRR	Ba
Lisbon	38.700	-9.183	5-15.2	Ba2, OL
Oeiras	38.683	-9.316	>6	Ba
Angra (Azores)	38.650	-27.216	?-14.6	Ba2
Huelva	37.250	-6.950	NRR	Ba
S. Vicente	37.000	-8.990	>10	Ba
Cádiz	36.533	-6.300	15-18.3	Ba, OL
Gibraltar	36.143	-5.353	2	Ba
Ceuta	35.888	-5.312	2	Ba
Tangier	35.766	-5.800	?-15.2	Ba, OL
Porto Santo	33.066	-16.330	3	Ba
Madeira	32.630	-16.880	4-13.2	Ba, OL
Safi	32.283	-9.233	>6	Ba
Canary Islands	28.135	-15.435	NRR	Re

Run-up reports from Baptista et al., 1998a (Ba1); Baptista et al., 2003 (Ba2); O'Loughlin and F. Lander, 2003 (OL); Ruffman, 1990, 2006 (Ru); Reid, 1914(Re)

Madeira, Lisbon, Angra and Tangier are bolded to indicate the large uncertainty regarding historical run-up amplitudes in those regions

NRR- Tsunami report but no run-up report

NR- No tsunami report

Table 2- Regions of reported tsunami run-ups (High) and regions where no run-ups were reported (Low)

	Far field	Near field
High run-up region	Caribbean	Lisbon to Morocco, Azores, Madeira
Low run-up region	U.S. East Coast	NW Spain

Table 3- Geographical coordinates of source locations shown in figure 3

Source Number	Latitude (°N)	Longitude (°E)
1	35.480	-8.200
2	36.210	-9.825
3	35.144	-10.055
4	37.150	-10.110
5	36.042	-10.753
6	37.045	-10.780
7	36.940	-11.450
8	36.015	-11.467
9	37.957	-12.052
10	36.835	-12.120
11	36.789	-13.039
12	36.300	-13.051
13	37.991	-13.414
14	37.205	-13.606
15	37.507	-14.514
16	36.748	-15.929

Source locations are measured in the center of each finite fault
 Bolded sources were rotated 360° and used to generate figure 15

Table 4- Fault parameters used for all simulations

Source Depth (Km)	Fault Length (Km)	Fault Width (Km)	Average Slip (m)	Dip (deg)	Rake (deg)
5	200	80	13.1	40	90

Source depth corresponds to the top of the fault plane

Table 5[Click here to download Table: Table 5new.doc](#)

Table 5- Comparison of historically observed tsunami arrival times with calculated arrival times from sources 5, 8 and 2 (S5, S8 and S2) in Figure 3 and compared to calculated arrival times from two sources (1 and 2) at the Marques de Pombal "source B"(N 160) and "source C" (N160N135) (Baptista et al., 1998b) and a source in the Gulf of Cadiz (Gutscher et al., 2006)

Location	Historical time	Travel time S5	Travel time S8	Depth (m)	Travel time S2	Depth (m)	Travel time MPF1	Travel time MPF2	Travel time GCF
St. Vincente	16 ± 7	16-17	21-22	4000-3500	16-19	1500-1000	25	21	22
Huelva	50 ± 10	39-44	45-51	2500-2000	39-47	1500-1000	80	74	52
Cadiz	78 ± 15	43-48	50-56	2500-2000	44-54	1500-1000	70	70	36
Gibraltar		52-58	59-66	2500-2000	55-68	1500-1000			53
Tangiers		48-53	54-61	2500-2000	50-62	1500-1000			54
Porto Santo	60 ± 15	48-51	44-47	4500-4000	58-62	4000-3500	68	70	59
Madeira	90 ± 15	54-57	49-52	4500-4000	64-68	4000-3500	78	78	72
Safi	26-34	35-37	37-39	4500-4000	37-40	4000-3500	75	81	55
Orieas	25 ± 10	34-38	37-42	2500-2000	38-47	2000-1500	28	22.6	51
Lisbon		35-39	38-43	2500-2000	39-48	1500-1000			
Figueira	45 ± 10	52-58	54-61	2500-2000	61-75	1500-1000	53	50	83
Porto		63-71	66-74	2500-2000	76-94	1500-1000	90	87.5	96

All times are in minutes.

Figure 1

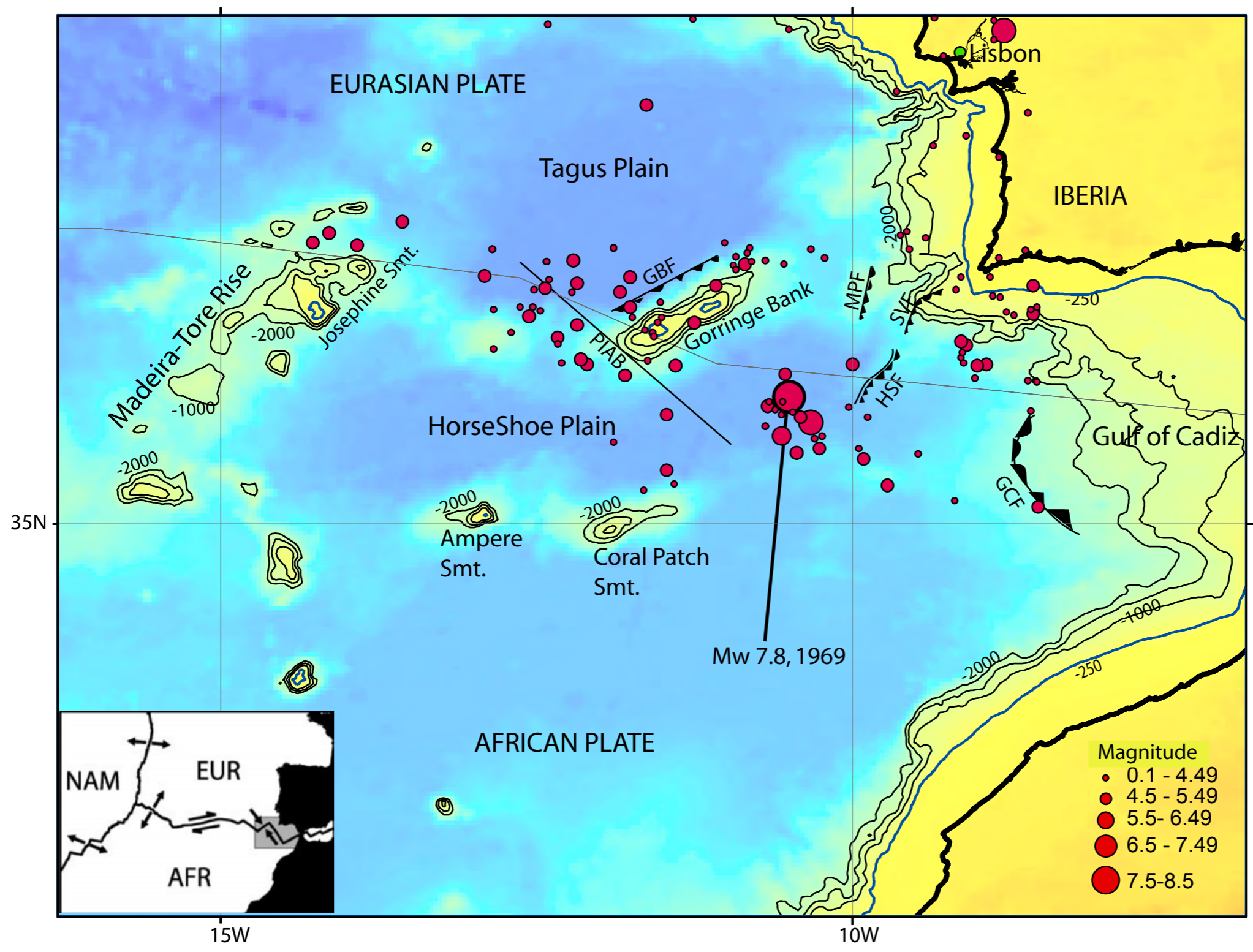


Figure 2

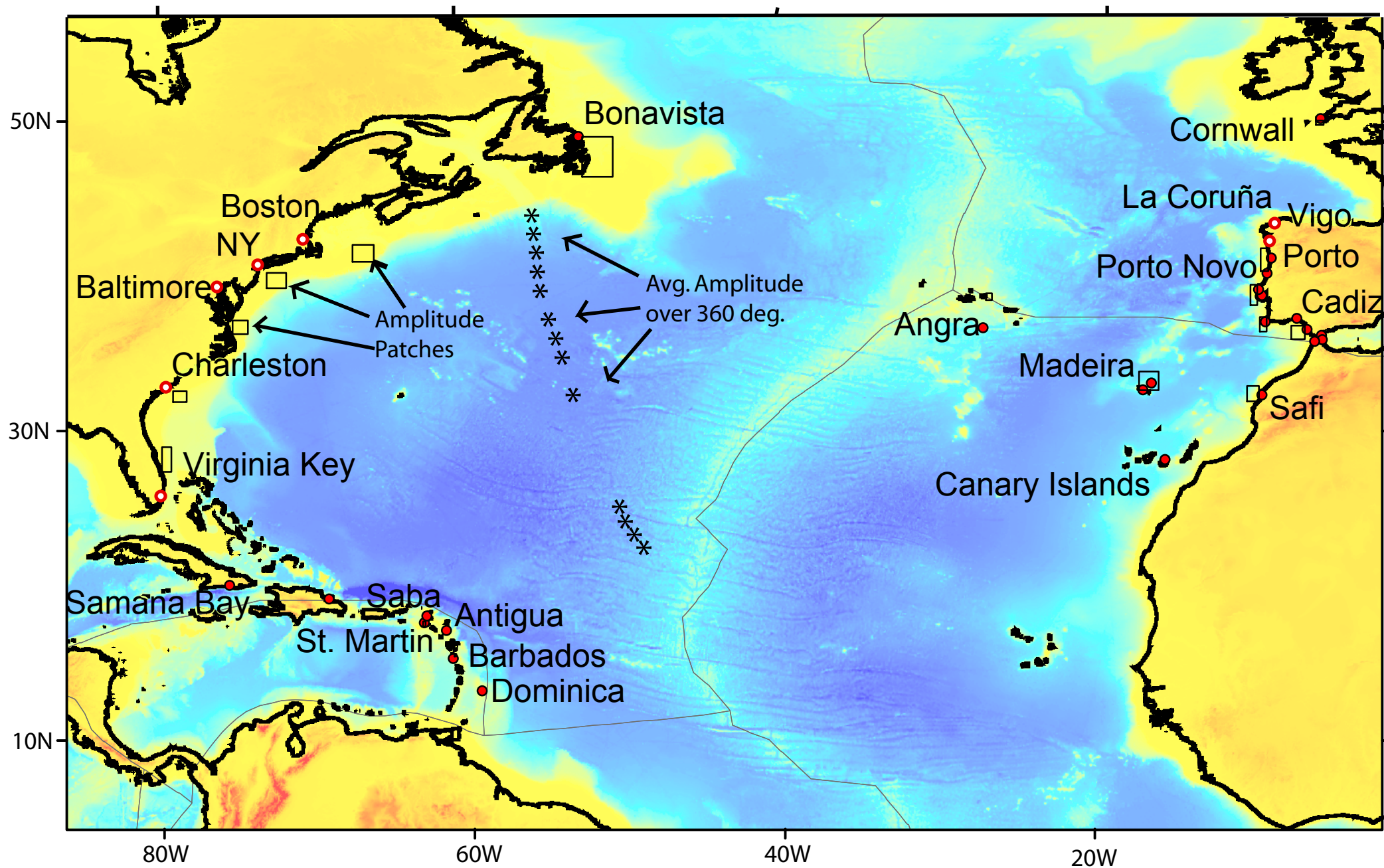


Figure 2.

Figure 3

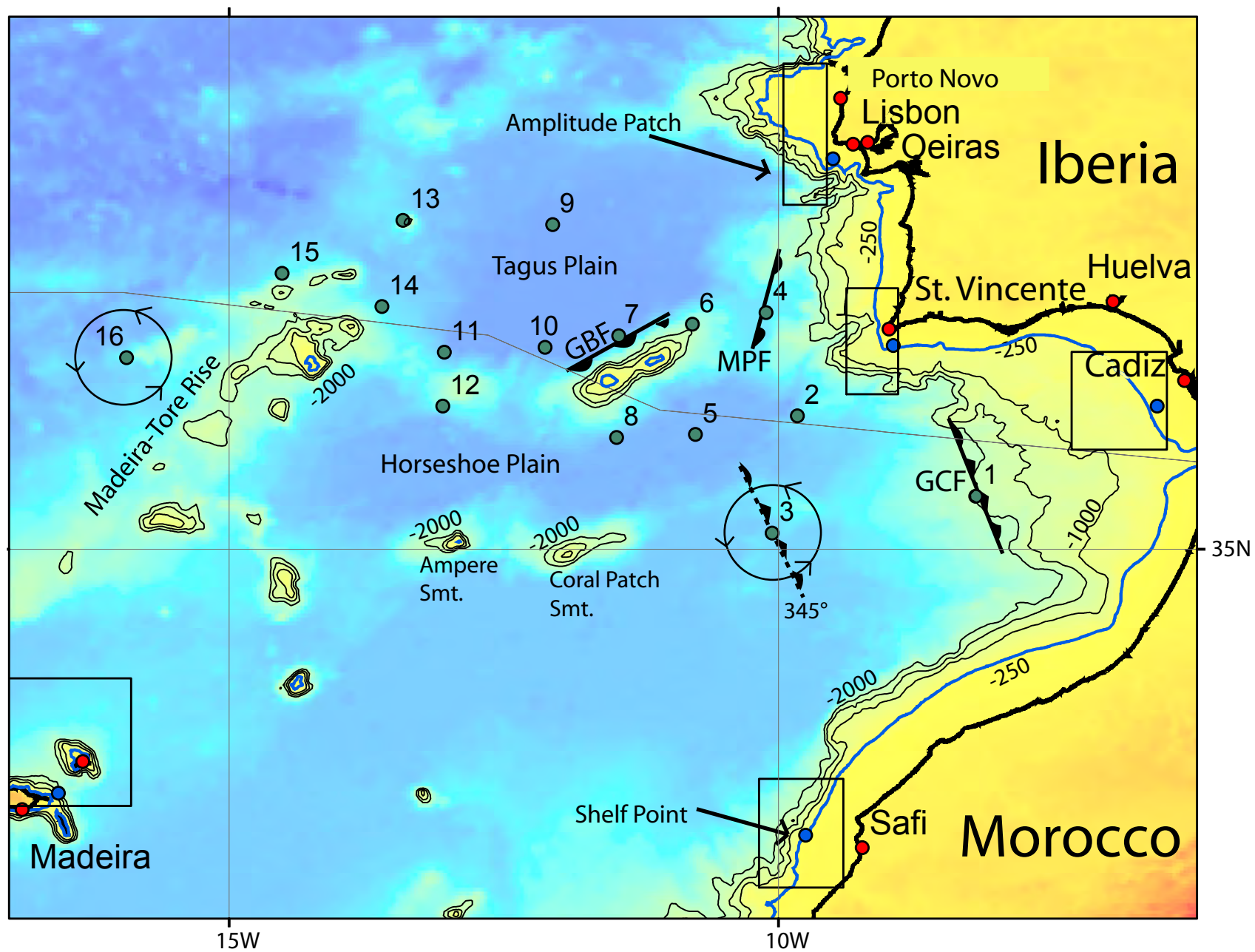


Figure 3

Figure 4

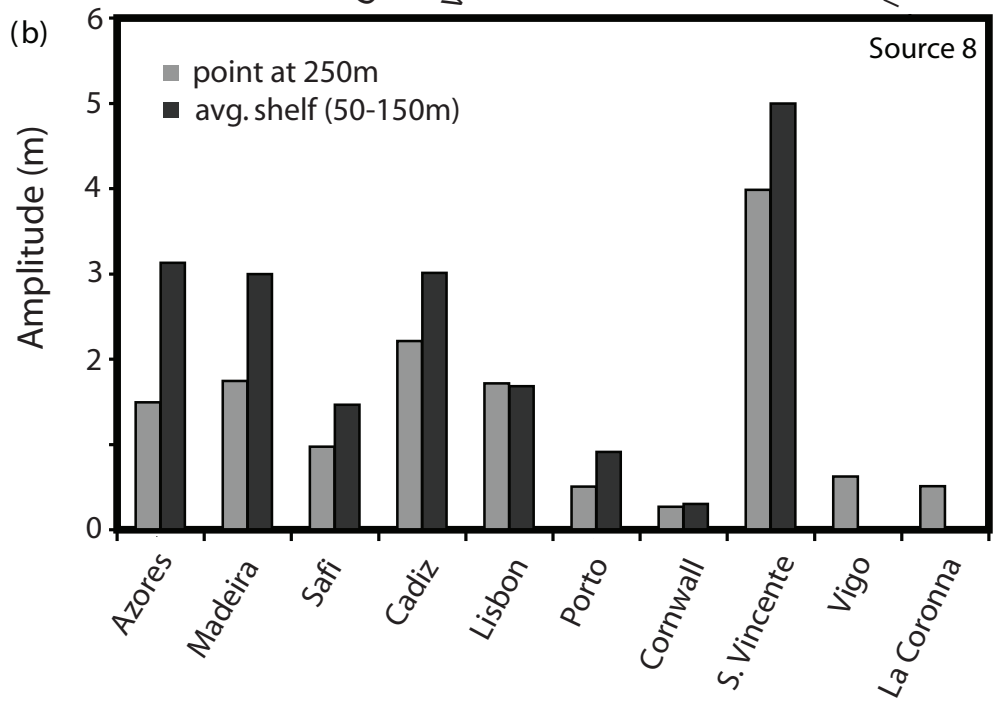
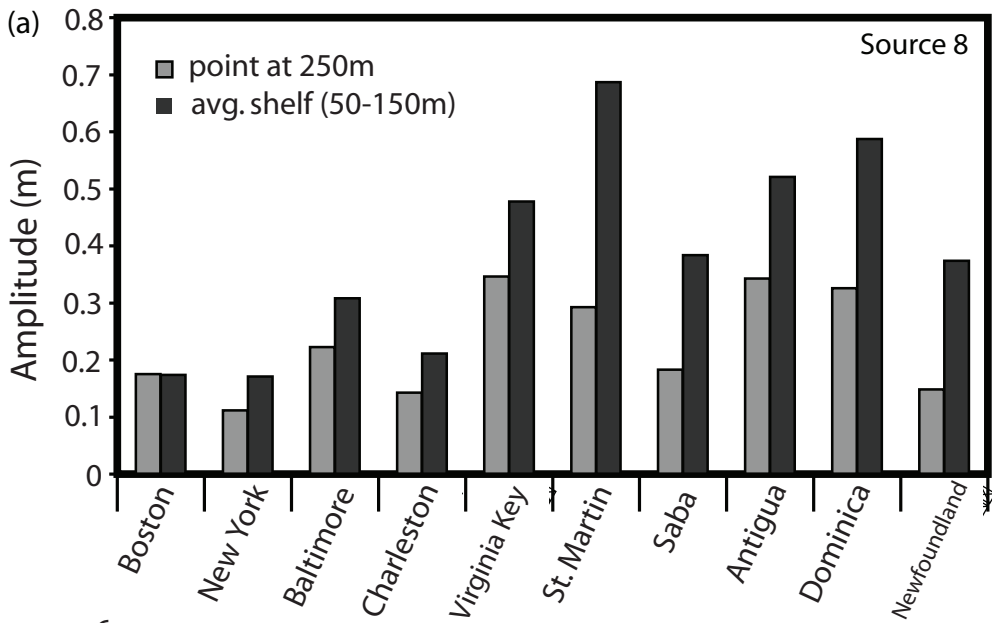


Figure 5

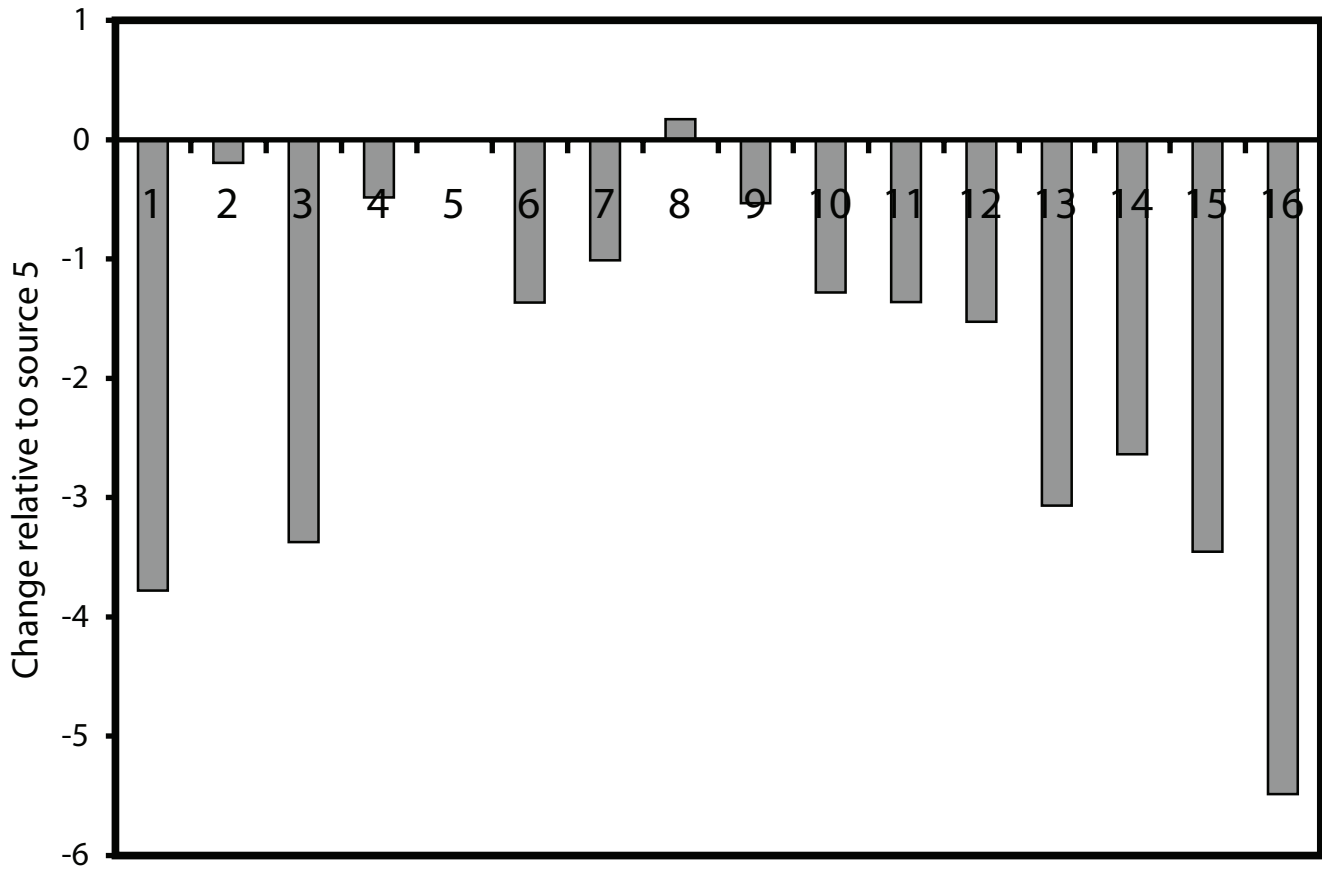


Fig. 6

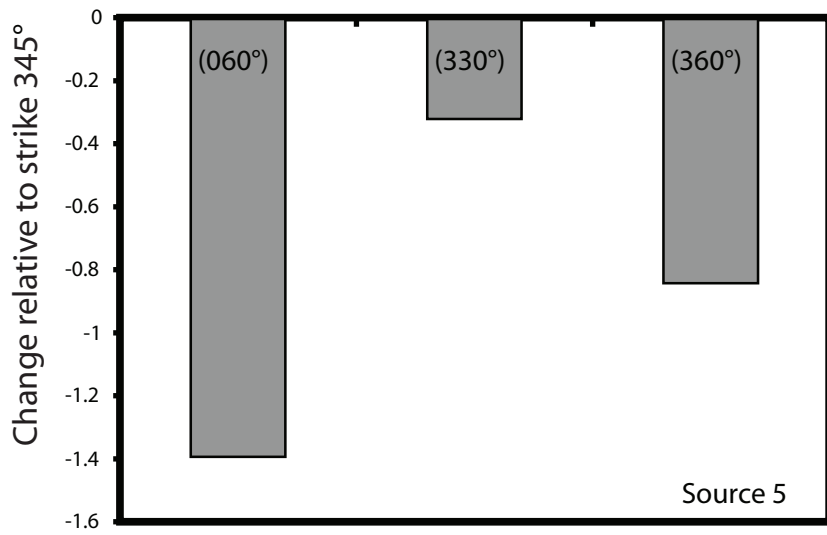


Fig. 7

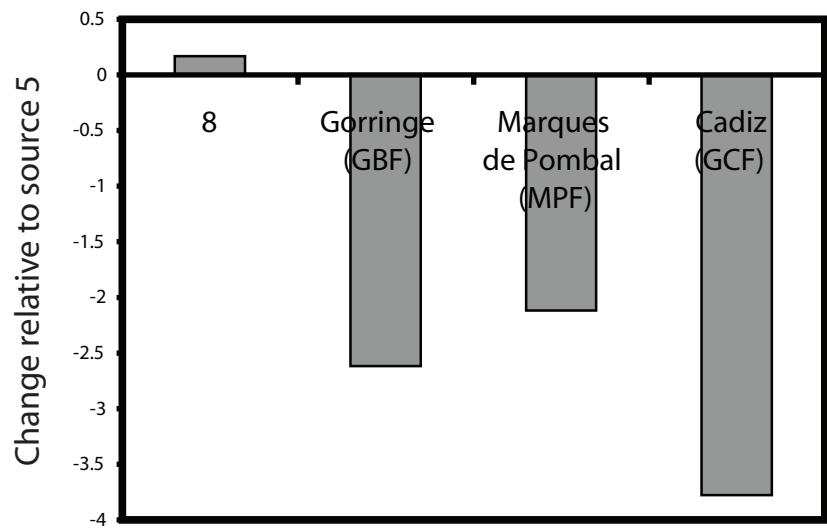


Figure 8

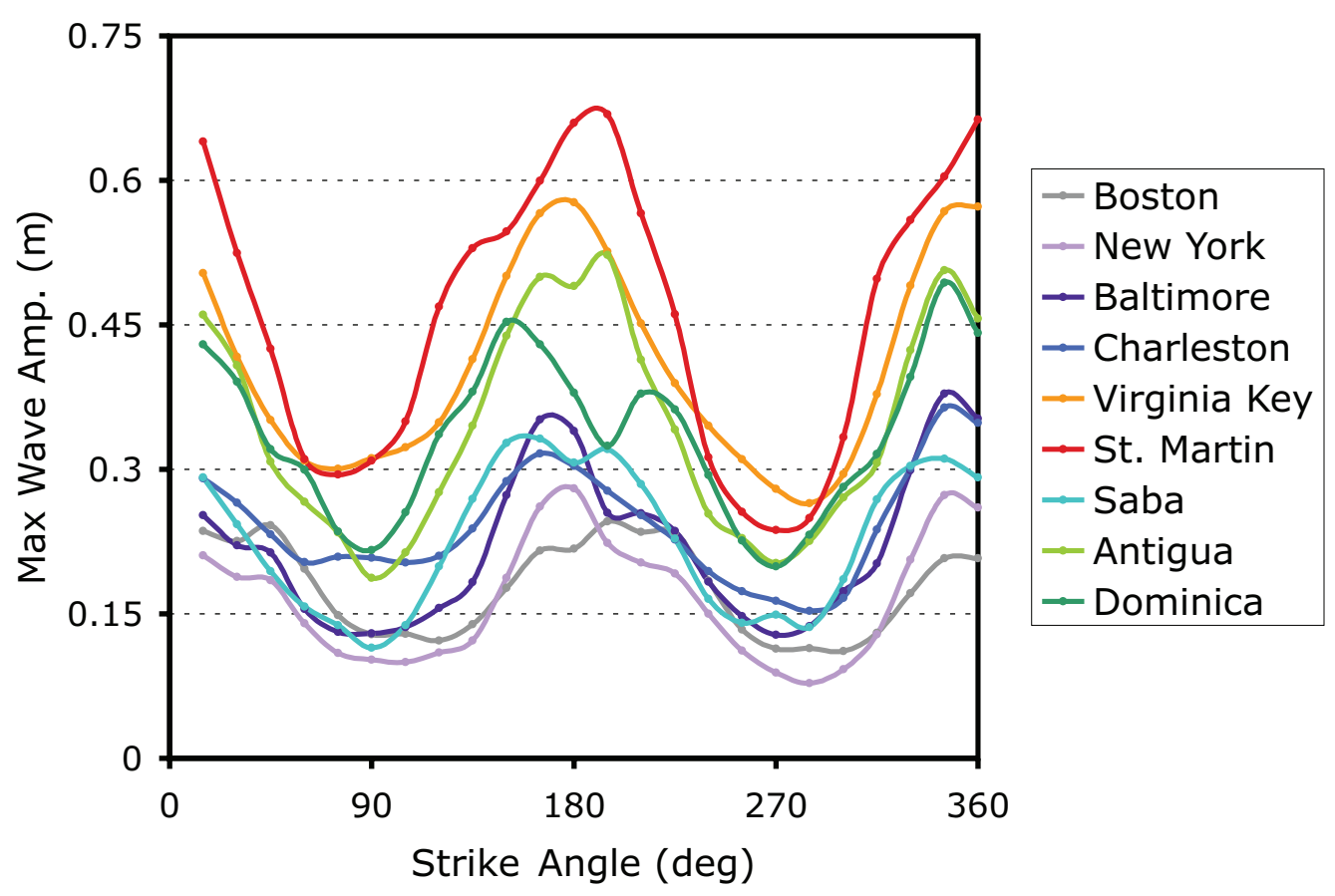


Figure 9

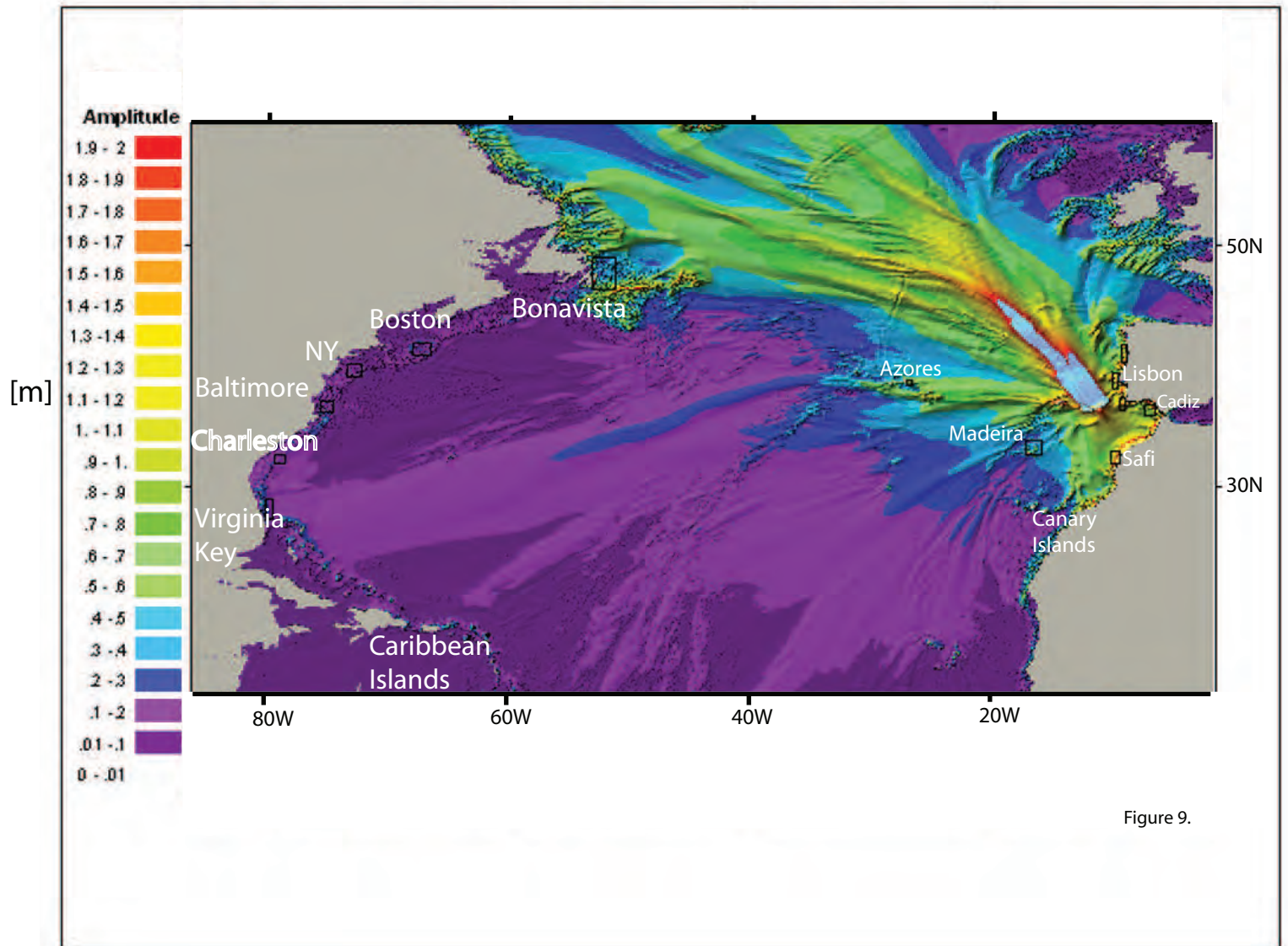


Figure 9.

Figure 10

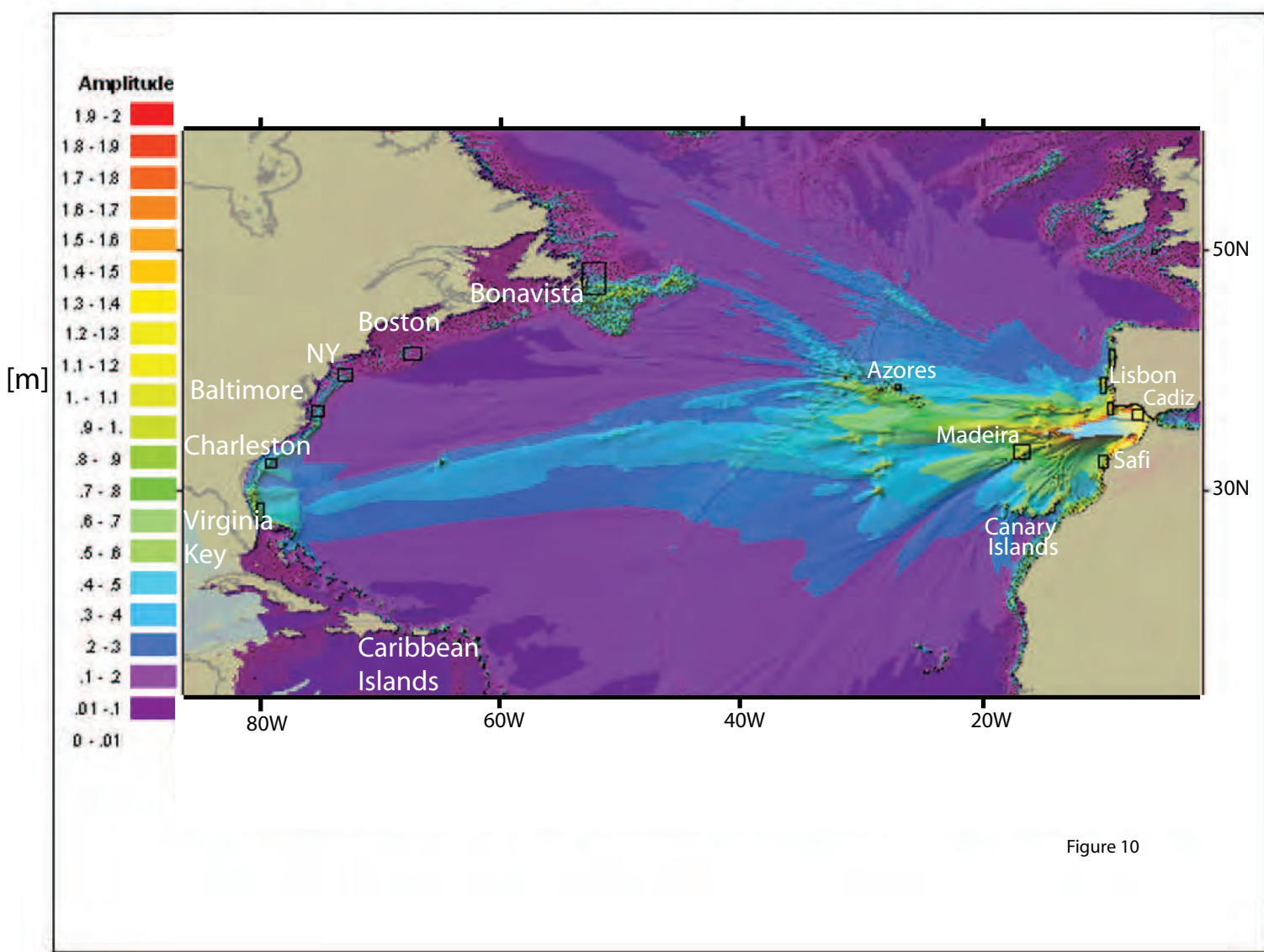


Figure 10

Figure 11

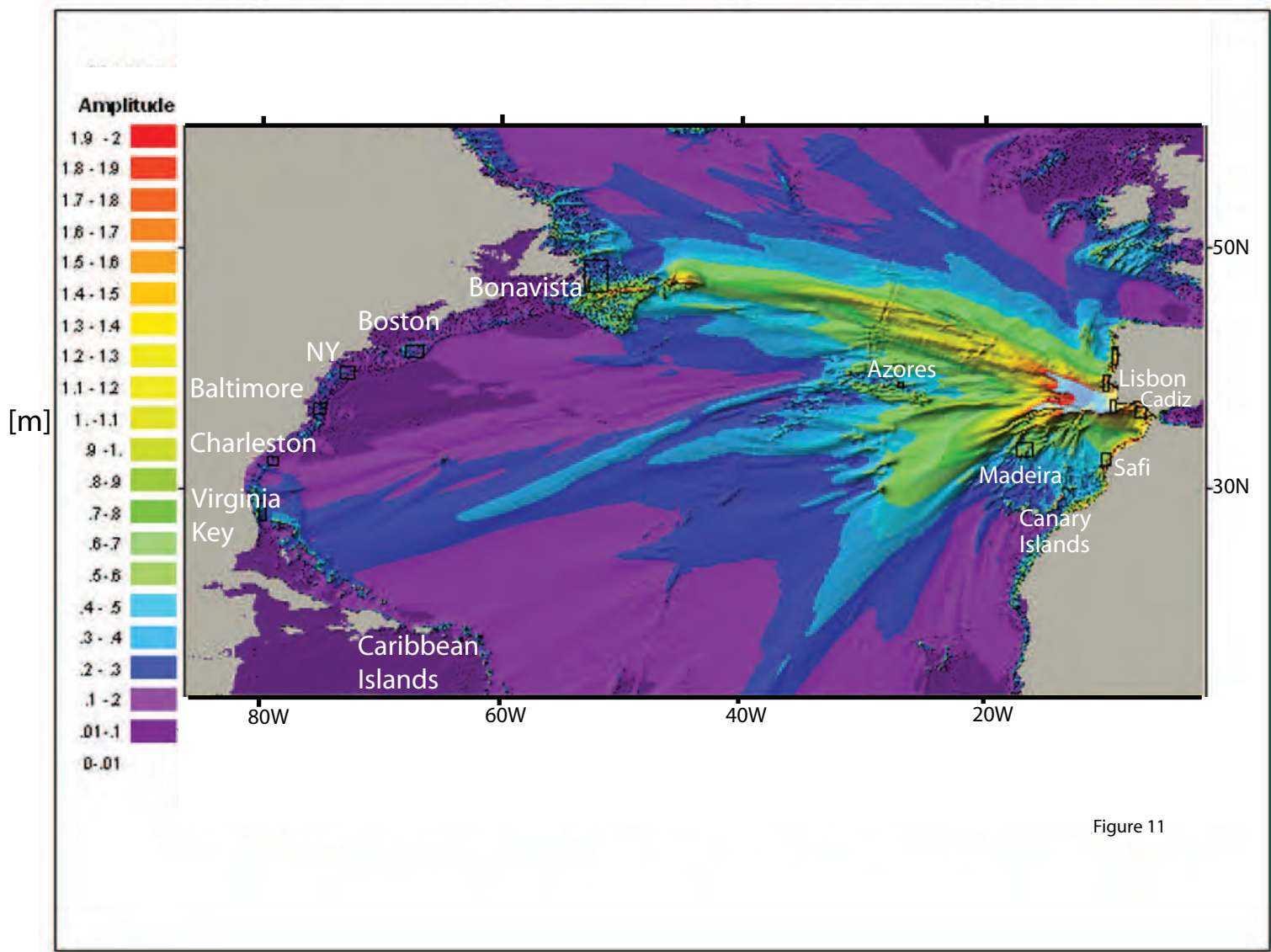


Figure 11

Figure 12

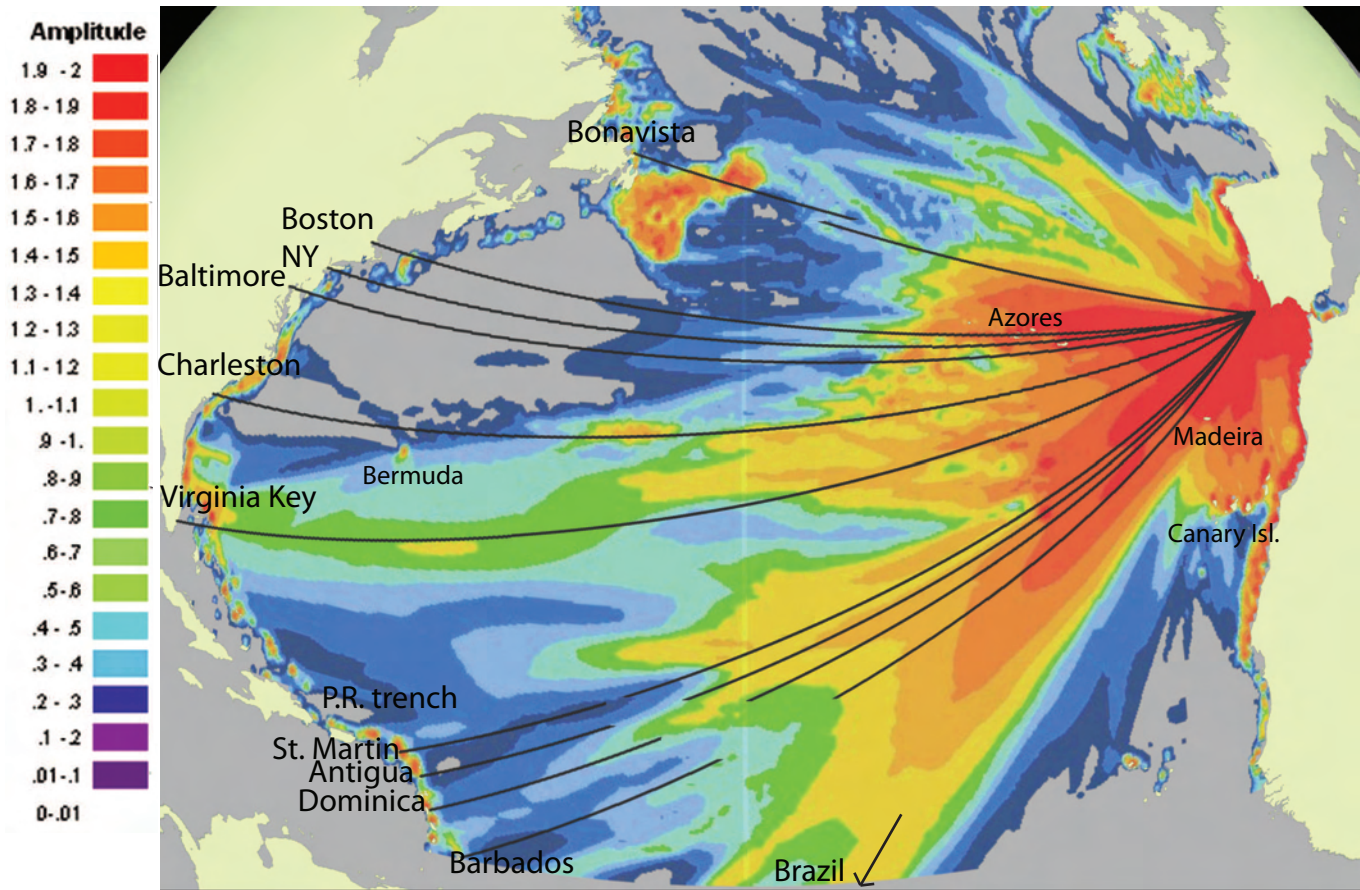


Figure 12.

Figure 13

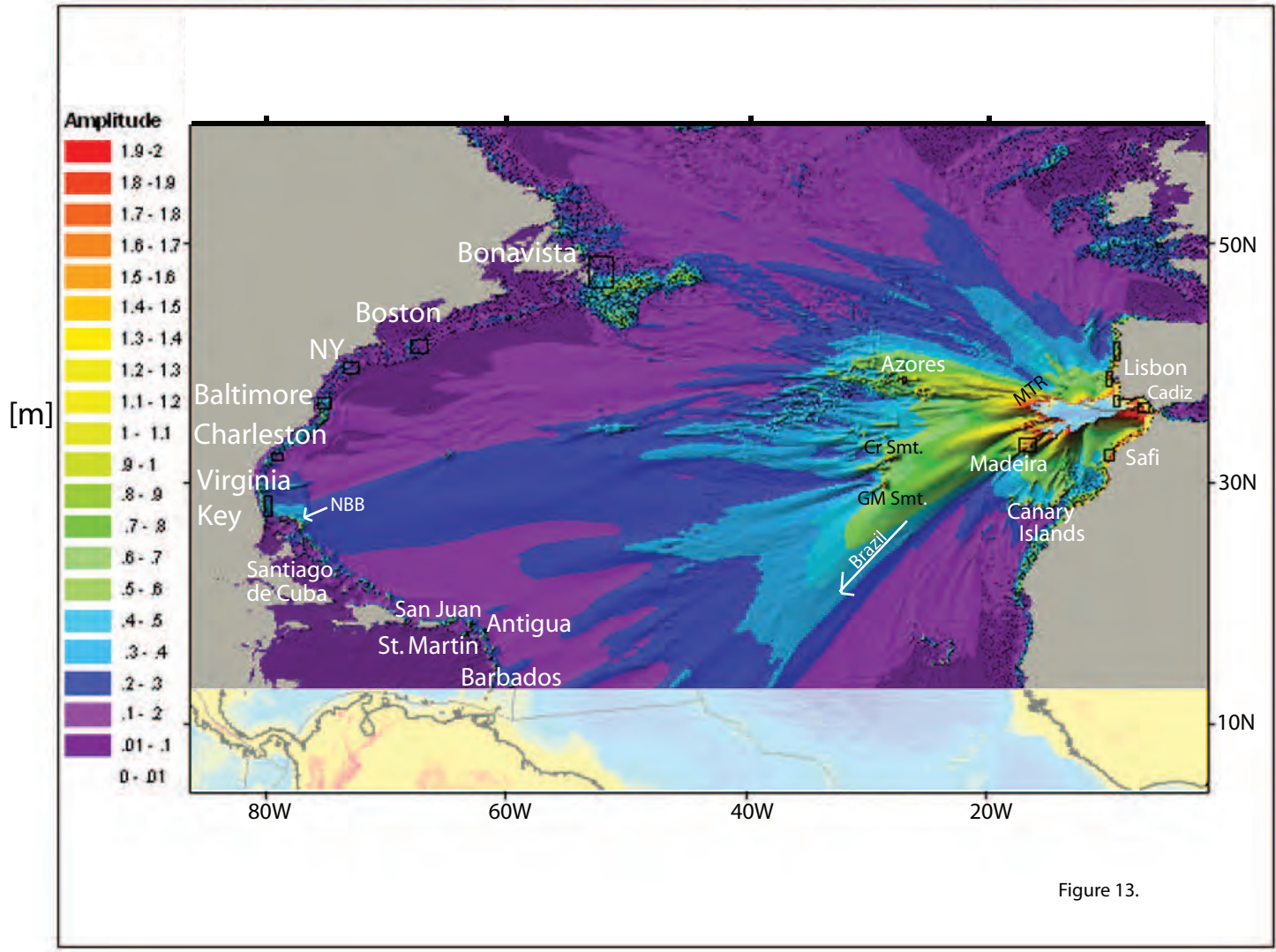


Figure 13.

Figure 14

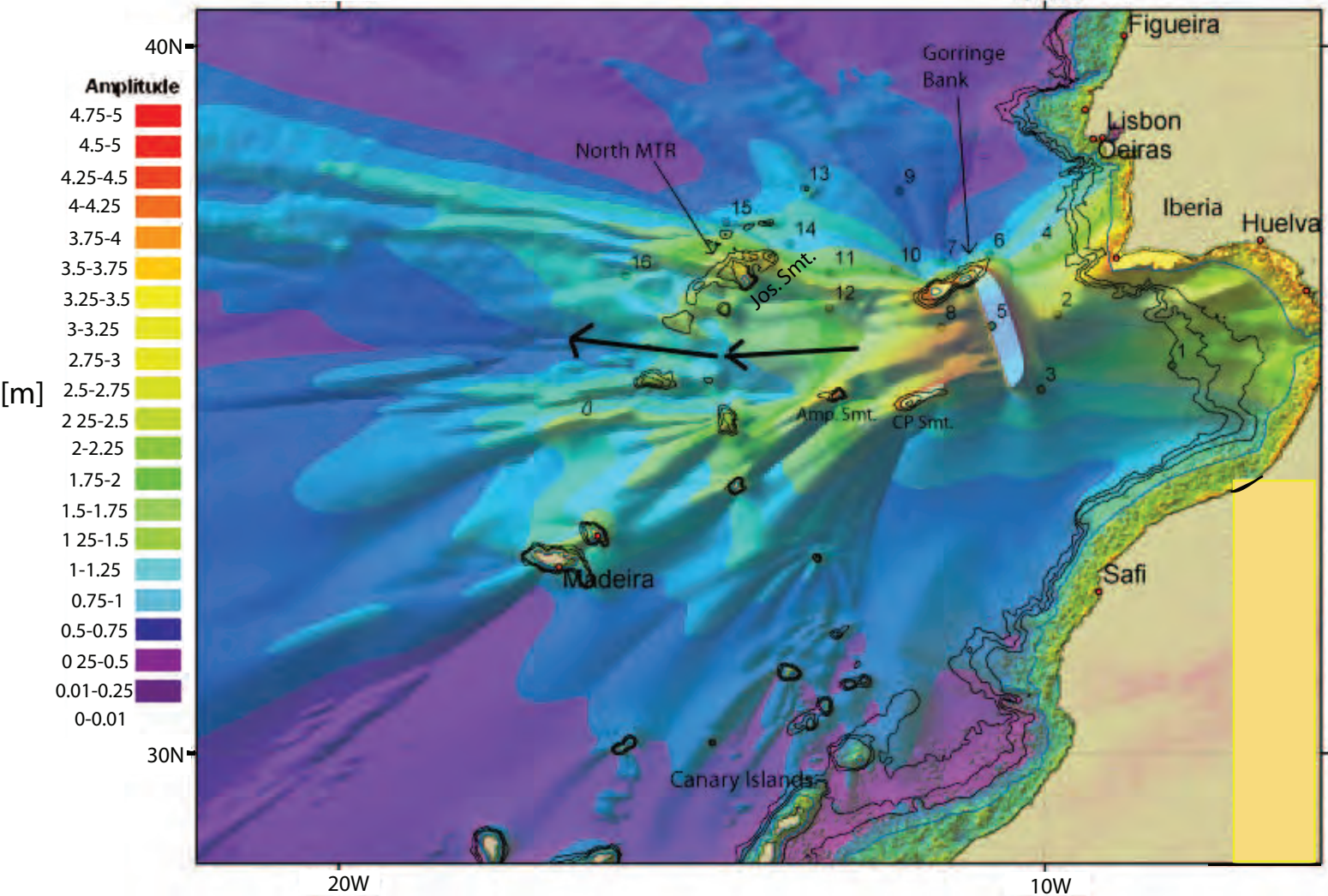


Figure 14.

Figure 15

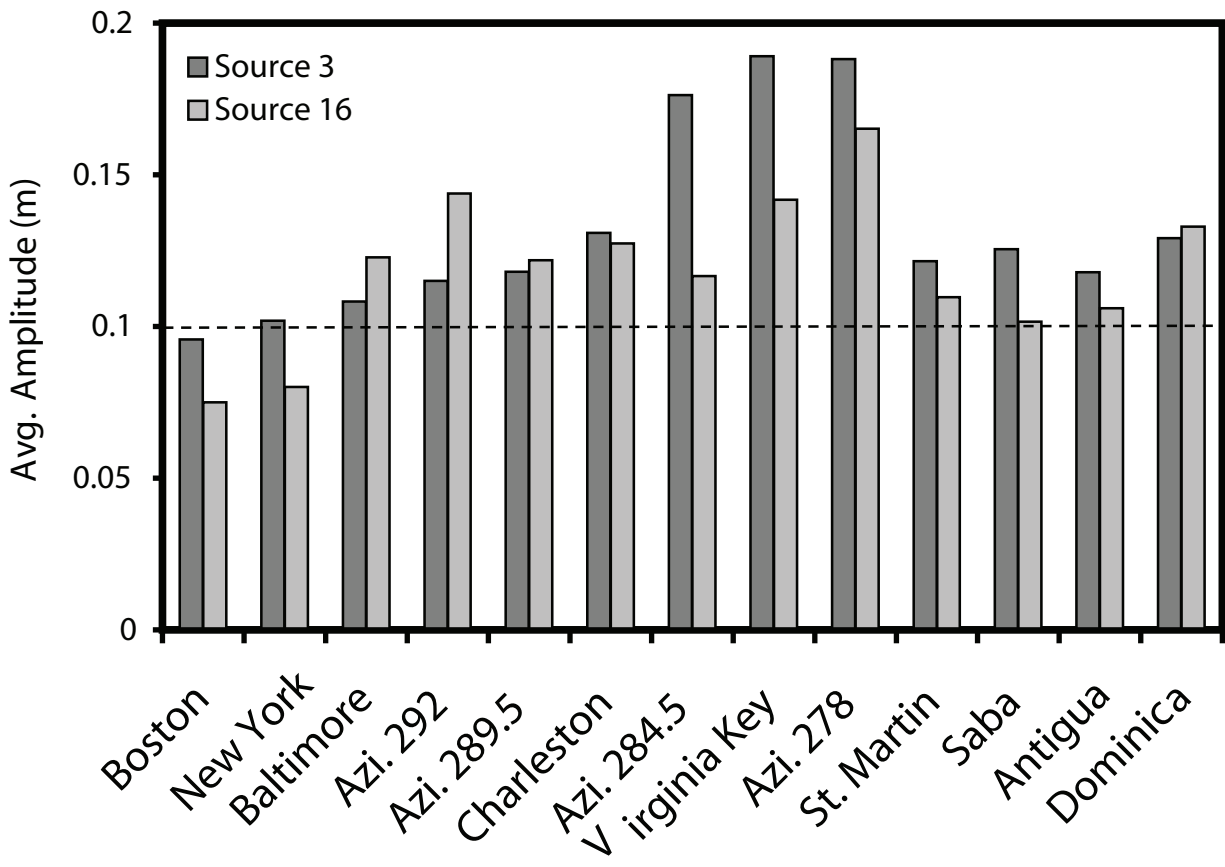


Figure 16

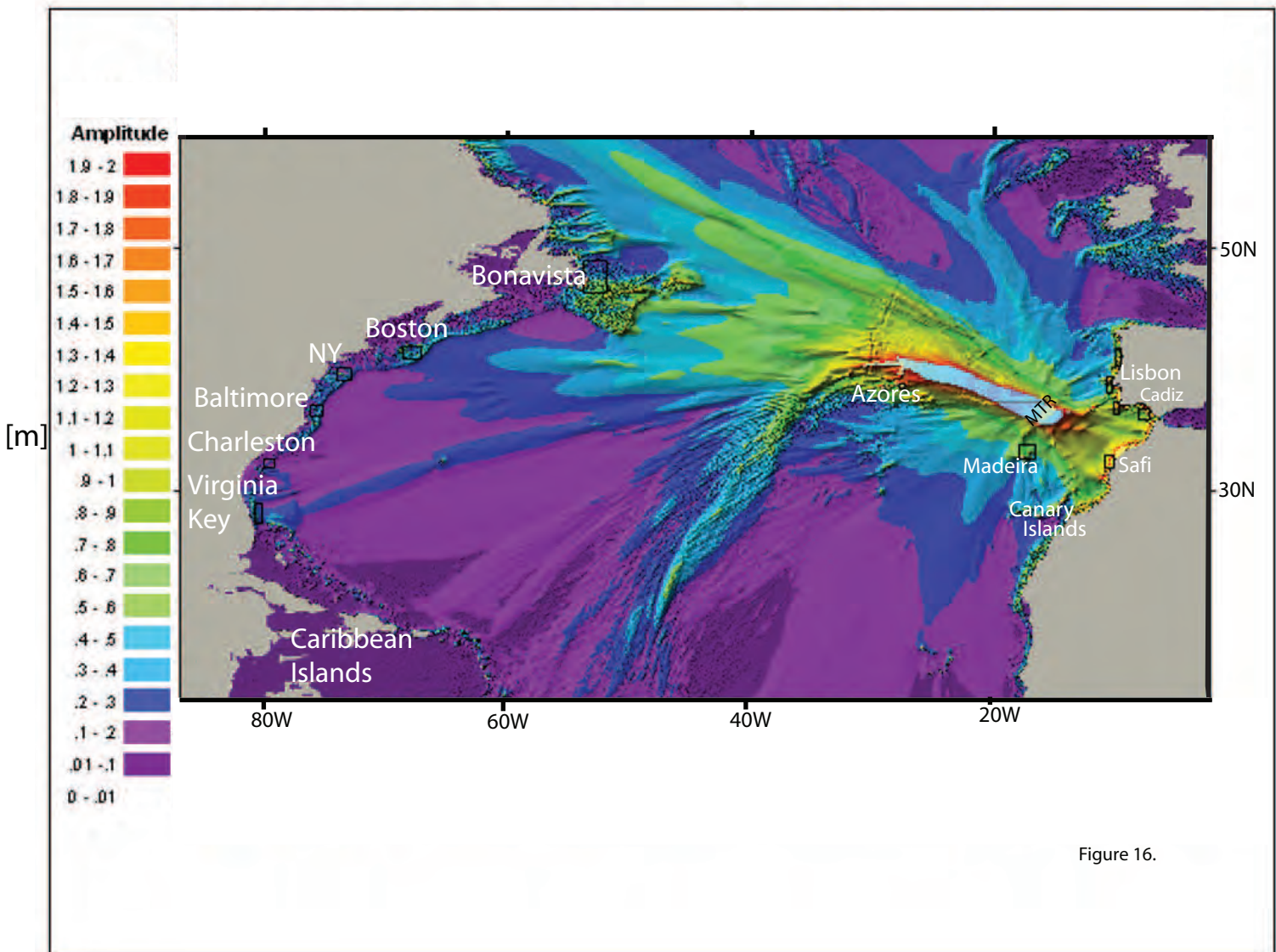


Figure 16.

Figure 17

